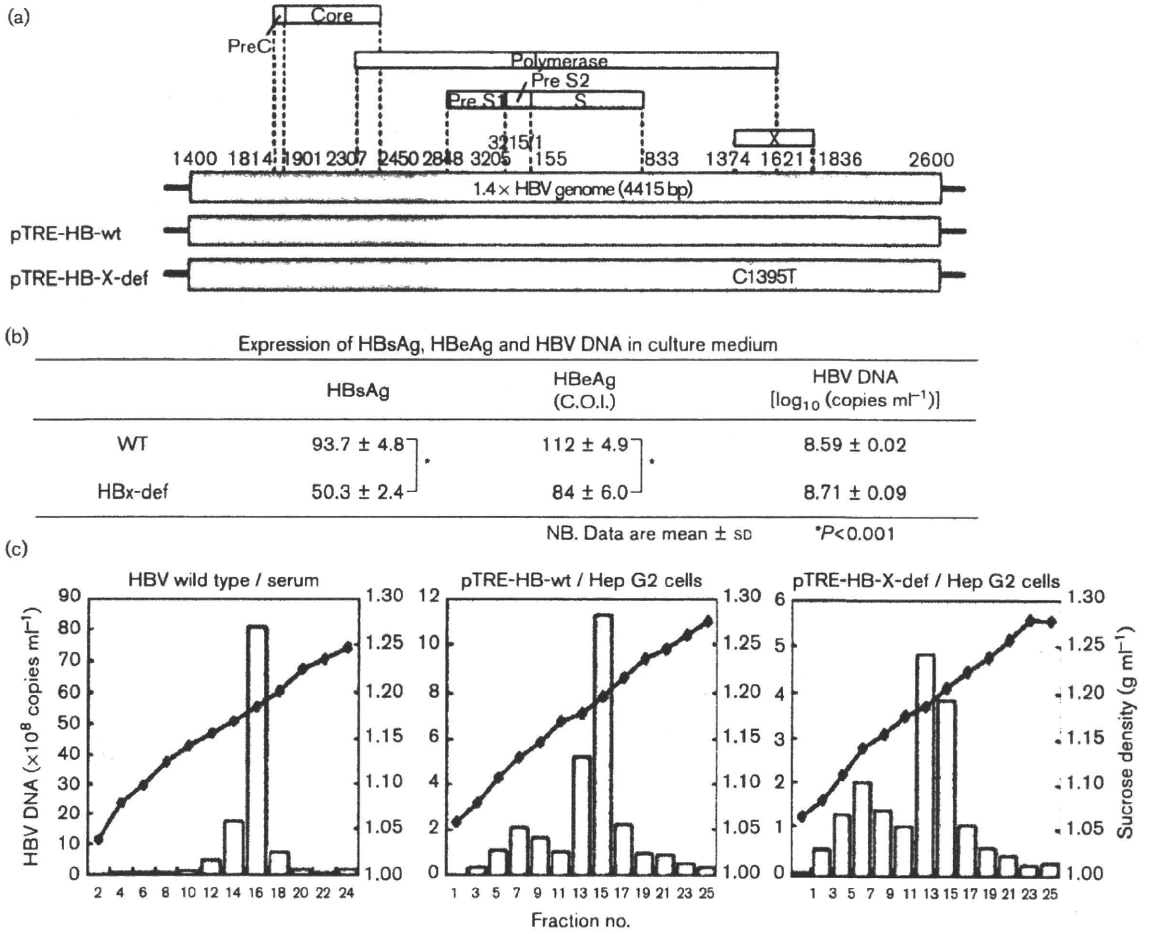

Fig. 1. Construction of HBV expression plasmids. (a) Wild type (WT) 1.4× genome length HBV was cloned into the pTRE2hyg vector (pTRE-HB-wt) and a nucleotide substitution, C1395T, was introduced to create the HBx-def mutant pTRE-HB-X-def. (b) Comparison of expression of HBsAg, HBeAg and HBV DNA in culture medium between WT and HBx-def. (c) Sucrose density gradient analysis of HBV particles (◆) and HBV DNA copies (bars) obtained from a serum sample (left) and supernatants from a cell culture transfected with WT HBV (pTRE-HB-wt, middle) and HBx-def pTRE-HB-X-def. C.O.I., cut-off index.

replication of HBV to the WT level. The effects of HBx protein were also evident on the expression of HBsAg (Fig. 3c) and HBeAg (Fig. 3d). As reported previously, the effect of the C-terminal two-thirds (aa 51–154) of the HBx protein was stronger than that of the entire protein and the N-terminal one-third (aa 1–50) (Tang *et al.*, 2005). The production of replication intermediates was increased similarly by co-transfection of the X proteins (Fig. 3e). To further study the effect of HBx expression, we analysed the levels of intracellular core protein expression. As shown in Fig. 4(a), the expression levels of the core protein were upregulated with the expression of the entire (WT) and C-terminal two-thirds (aa 51–154) of the HBx protein. Immunocytochemical analysis showed that only the cells with strong HBx protein expression were stained with the core protein (Fig. 4b). The core and HBx proteins in these cells were stained mainly in the cytoplasm.

Expression of HBx protein in mouse liver by hydrodynamic injection

Next, we expressed the HBx protein in the chimeric mouse liver with hydrodynamic injection. As shown in Fig. 5(a), a dose-dependent expression of the HBx protein with a haemagglutinin (HA) tag was confirmed by Western blot analysis. Although Henkler *et al.* (2001) showed an aggregation of HBx under the control of the human cytomegalovirus (CMV) promoter, we were able to observe expression of properly sized HBx. Immunohistochemical analysis also revealed HBx protein expression in the mouse

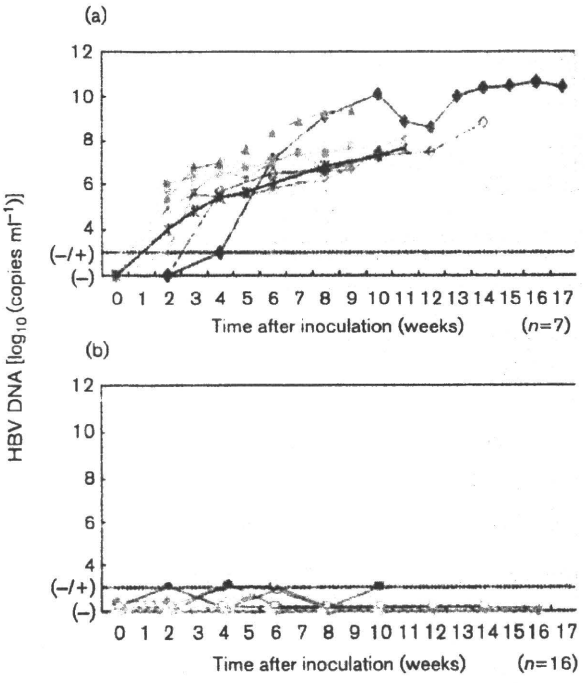

No. analysed mice

Weeks		2	4	6	8	10	12	14	16
HBV	(−/+)	1	3	3	0	1	0	0	0
DNA	(−)	15	10	6	9	6	5	5	3

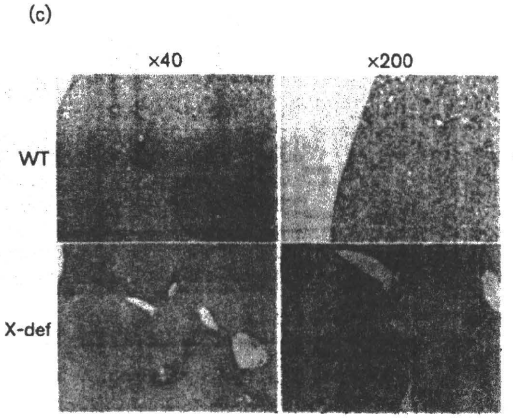

Fig. 2. Infection of human hepatocyte chimeric mice with cell-culture-derived HBV. (a, b) WT (a) and HBx-def (b) HBV particles generated from HepG2 cell lines by transfection of overlength HBV plasmid injected into chimeric mice. (c) Immunohistochemical analysis of mouse liver infected with WT (upper panel) and HBx-def (lower panel) HBV using anti-HBc antibody. HBV-infected hepatocytes were stained brown.

liver. Notably, the HBx protein staining was strong around the central vein (Fig. 5b).

Infection of HBx-def HBV particles with intrahepatic expression of the HBx protein

As the infection experiments with HBx-def HBV failed to result in measurable viraemia (Fig. 2b), we then tried to infect HBx-def HBV after expression of HBx protein by hydrodynamic injection. As shown in Fig. 6(a), six of seven mice developed measurable viraemia 2–8 weeks after inoculation. The incidence of measurable viraemia was significantly higher in mice that received hydrodynamic injection than in those without (Fig. 2b versus Fig. 6a, $P<0.0001$). Immunohistochemical analysis of the infected mice showed simultaneous staining for human serum albumin (hAlb) and HBcAg in the same portion of the liver (Fig. 6b).

Sequence analysis of inocula and the infected mouse sera

We analysed nucleotide sequences of the virus recovered from all six infected mice and compared them with those of inoculated HBx-def HBV. As shown in Fig. 7(a), direct sequencing analyses of the amplified HBV DNA products showed that all revertant viruses had T1395C (mouse MHX#1, 3, 5–7) or T1395A (mouse MHX#2) point mutations, which reverted the introduced stop codon to amino acids. We further analysed nucleotide sequences of HBV by cloning and sequencing using serum samples obtained from two mice (MHX#1, 33 clones; MHX#2, 38 clones) (Fig. 7b). Only one of 33 clones obtained from MHX#1 and none of the 38 clones from MHX#2 had the stop codon mutation that was introduced into the transfected plasmid.

DISCUSSION

In previous studies, HBx has been reported to be a multifunctional protein affecting cell growth and proliferation and activating transcription of mRNA (Arbuthnot *et al.*, 2000; Bouchard *et al.*, 2001; Klein *et al.*, 1999; Murakami, 2001) and virus replication in HCC cell lines (Bouchard *et al.*, 2001; Keasler *et al.*, 2007; Leupin *et al.*, 2005; Tang *et al.*, 2005) and mouse hepatocytes (Keasler *et al.*, 2007; Xu *et al.*, 2002). However, these results were obtained by introduction of HBV genomes into cells using artificial methods such as transfection, gene transfer and hydrodynamic injection. Recently, we established an *in vivo* HBV infection system using human hepatocyte chimeric mice (Tsuge *et al.*, 2005). The system enabled us to perform infection experiments using HBV-containing patient sera and cell-culture medium. Using this system,

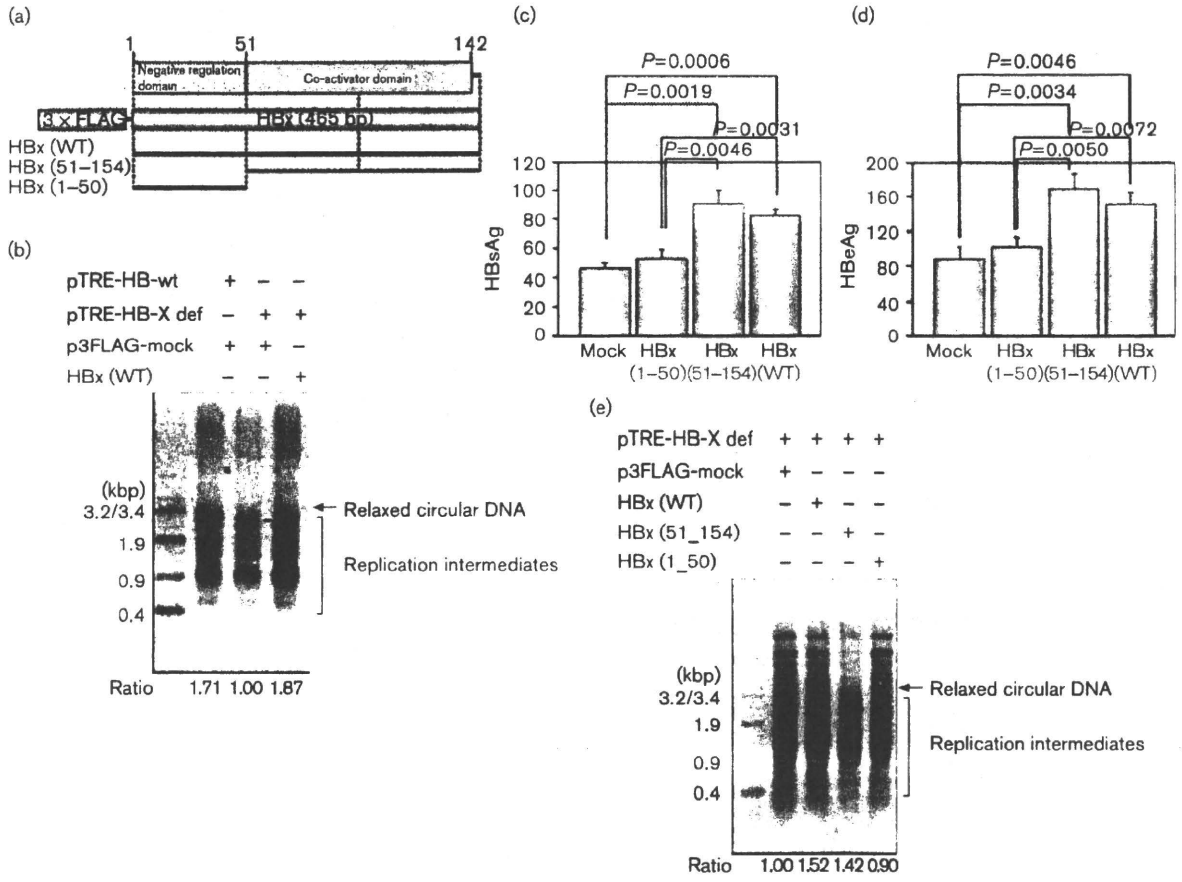

Fig. 3. Recovery of reduced formation of replication intermediate and HB antigens from HBx-def HBV by *trans*-complementation of HBx. (a) Construction of HBx expression plasmids. Full-length and deletion mutants of HBx gene were cloned into the p3FLAG-CMV10 or pcDNA3 or pcDNA3.1-3HA vector. Examples of three FLAG-tagged plasmids are shown. (b) *Trans*-complementation of HBx protein restored the reduced formation of replication intermediates of HBx-def HBV. The core-associated HBV replication intermediates were collected from HepG2 cells and detected with Southern blot hybridization with a full-length HBV probe. (c–e) Recovery of reduced production of HBsAg (c) and HBeAg (d) in culture medium and replication intermediates (e) of HBx-def HBV with *trans*-complementation of HBx expression plasmids. HBx (WT) and HBx(51–154), but not HBx(1–50), effectively enhanced the formation of HBV products. (b, e) The levels of core-associated HBV DNA are shown at the bottom of each lane. Data in (c) and (d) are mean ± SD of three experiments.

we showed previously that HBeAg is dispensable for HBV infection and active replication *in vivo* (Tsuge *et al.*, 2005). Virus replication following infection of HBV particles is quite similar to natural infection. We thus applied the system to study the function of HBx protein in this study. We also utilized hydrodynamic injection of HBx expression plasmid to *trans*-complement the defective HBx. As shown by Western blot analysis (Fig. 4a), HBx protein of the expected size was produced without development of antibody in this SCID-mouse-based model system.

This natural infection mode is quite different from previous animal studies. Virus titres of HBx-def HBV were approx. 50–99 % compared with WT HBV *in vitro* (Bouchard *et al.*, 2001; Keasler *et al.*, 2007; Leupin *et al.*, 2005; Tang *et al.*, 2005) and *in vivo* (Keasler *et al.*, 2007; Xu *et al.*, 2002). High-level HBx-def virus production seen in these experiments may be the result of expression of HBV proteins other than HBx following forced introduction of plasmids into mouse liver cells by hydrodynamic injection or transgenes. Such introduction probably resulted in virus production that is similar to *in vitro* transfection experiments using cultured cells.

In vitro experiments in this study showed that normal-density HBV particles (Fig. 1c) were produced in the absence of HBx. Curiously, the amount of HBV DNA released from the cells into the supernatant was not different between WT and HBx-def HBV, even though the

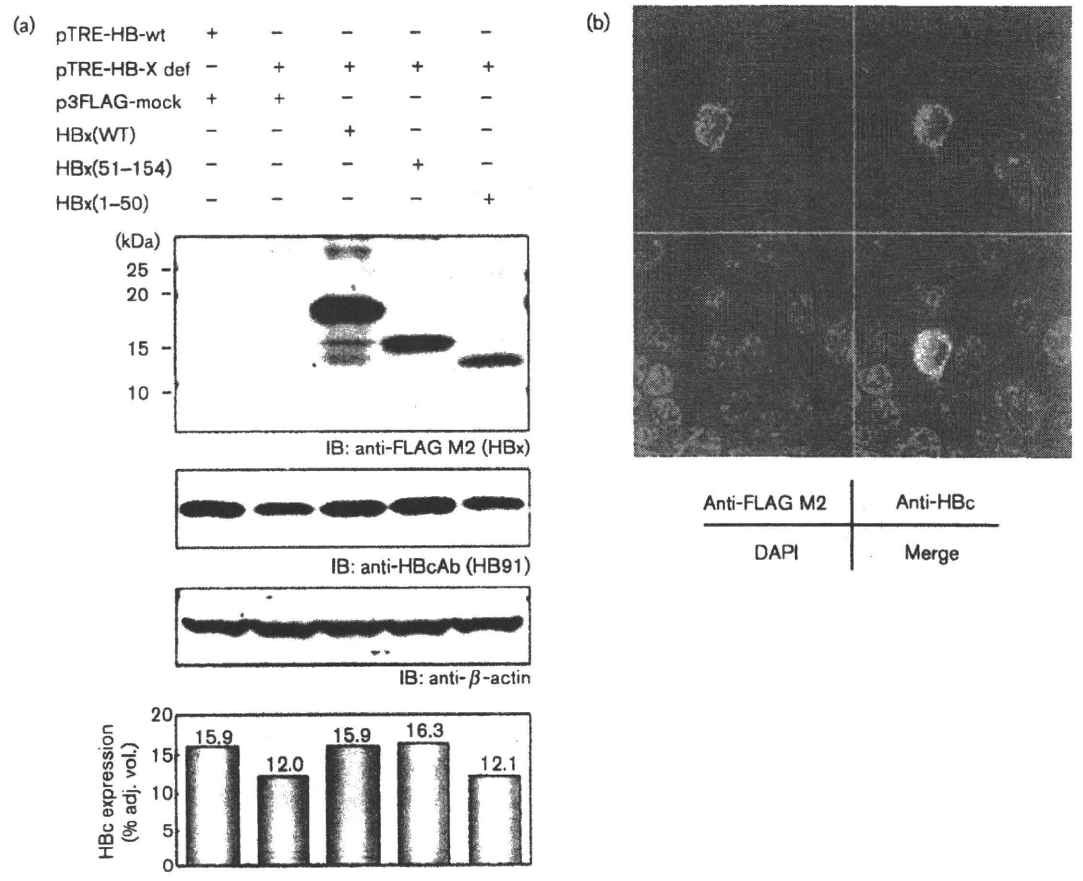

Fig. 4. Upregulation of intracellular core protein formation by *trans*-complementation of the HBx proteins. (a) Western blot analysis of intracellular proteins. Expression of the HBx proteins (percentage adjusted volume) is shown by staining the fused FLAG tag (upper panel). The membrane was also stained by the anti-HBc (middle) and anti-β-actin (lower) antibodies. Values obtained by scanning via densitometer are shown at the bottom of each lane. (b) Immunohistochemical analysis of HepG2 cells co-transfected with pTRE2-HB-X-def and p3FLAG-HBx plasmids. The expression of HBx and HBc proteins was detected by anti-FLAG (upper left) and anti-HBc (upper right) antibody, respectively. The merged image is shown in the lower right and nuclei are shown in the lower left panel. Note that only cells positive for HBx are also positive for HBc protein.

amounts of HBsAg and HBeAg as well as the amount of HBV DNA in cells were significantly greater in WT (Fig. 1b). Efficacy of release of the virus from the cells might be different between WT and HBx-def HBV. Alternatively, production of defective virus, which appeared as the second peak of HBV DNA in the sucrose gradient experiment (Fig. 1c, right panel), might be enriched in HBV DNA in the supernatant of HBx-def HBV. The reason for this discrepancy is unknown. Previous papers did not mention such production of HBV into the supernatant.

Similarly, in the absence of HBx protein *in vitro*, the formation of the replication intermediates (Fig. 3) and production of intracellular core protein (Fig. 4) continued, although their amounts were much lower. It is thus difficult to explain the inability of HBx-def HBV to infect *in vivo* simply from its transcription-activating ability, although our results confirmed that HBx has *trans*-activation ability, as reported previously (Keasler *et al.*, 2007; Tang *et al.*, 2005; Xu *et al.*, 2002). A different mode of introduction of viral nucleic acid might explain the difference seen in *in vitro* and *in vivo* experiments. In the transfection experiments, a relatively large amount of HBV DNA is introduced by transfection. In contrast, only successfully attached virus particles can introduce viral DNA into liver cells.

Strikingly, all but one (70 of 71 clones) revertant viruses had nucleotide substitutions that reversed the introduced stop codon to a coding amino acid. This is in contrast to the fact that HBV replicates in the HBx-def form in cultured cells, even though the efficacy is lower than in WT. We assumed that complemented HBx protein stimulated the replication of HBx-def HBV and increased the chance of nucleotide sequence substitutions in the HBx

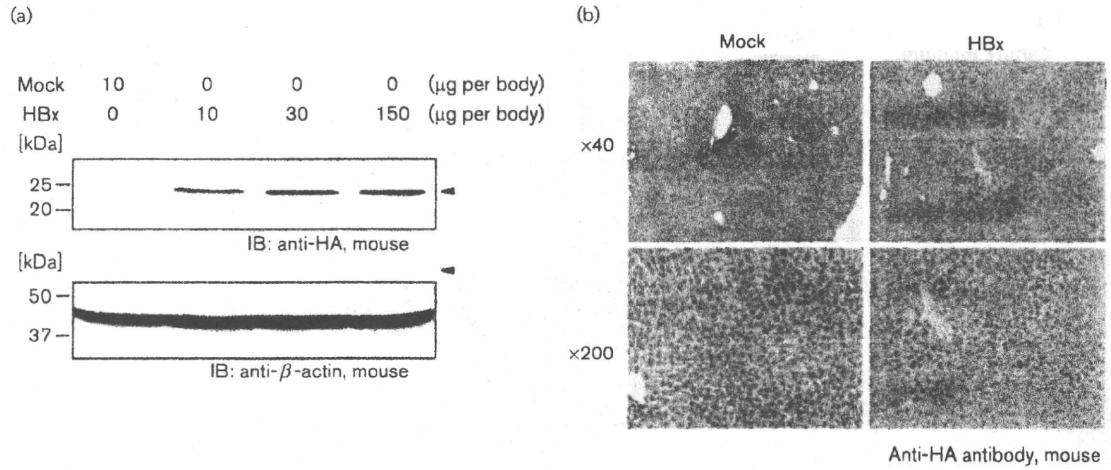

Fig. 5. Expression of HBx protein by hydrodynamic injection of HBx plasmid. (a) Liver-expressed HA-tagged HBx proteins were detected by Western blot analysis using anti-HA antibody (HA tag was used to avoid non-specific binding of anti-FLAG tag to mouse liver proteins). Dose-dependent expression of the protein was observed with different doses of the injected plasmid. (b) Immunohistochemical analysis of mouse liver using anti-HA antibody revealing expression of HBx protein. The protein was mainly expressed around the central vein.

gene, and that only revertant HBV variants predominantly increased, due to their rapid replication ability through the infection–replication cycle that only exists in the *in vivo* model. One might consider the possibility that the HBx protein works as a mutagen. However, we did not observe clear differences in the incidence of nucleotide sequence substitutions between the presence and absence of HBx (Fig. 7b and data not shown).

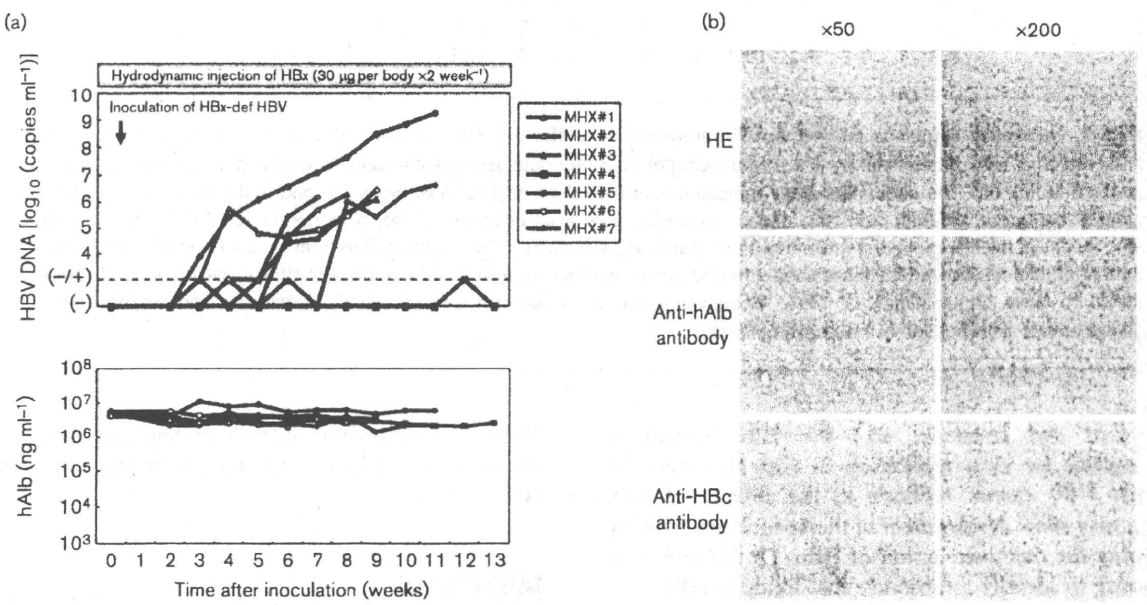

Fig. 6. Infection of HBx-def HBV particles after hydrodynamic injection of HBx expression plasmid. (a) Full-length HBx protein expression plasmid was hydrodynamically injected twice a week into human hepatocyte chimeric mice. Two weeks after the beginning of the injections, cell-culture-derived HBx-def HBV particles were injected through the tail vein. HBV DNA (upper panel) and hAlb (lower panel) were measured. (b) Immunohistochemical analysis of the infected mouse. The liver was stained with haematoxylin and eosin (HE) (upper), antibody against hAlb (middle) and anti-HBc antibody (lower).

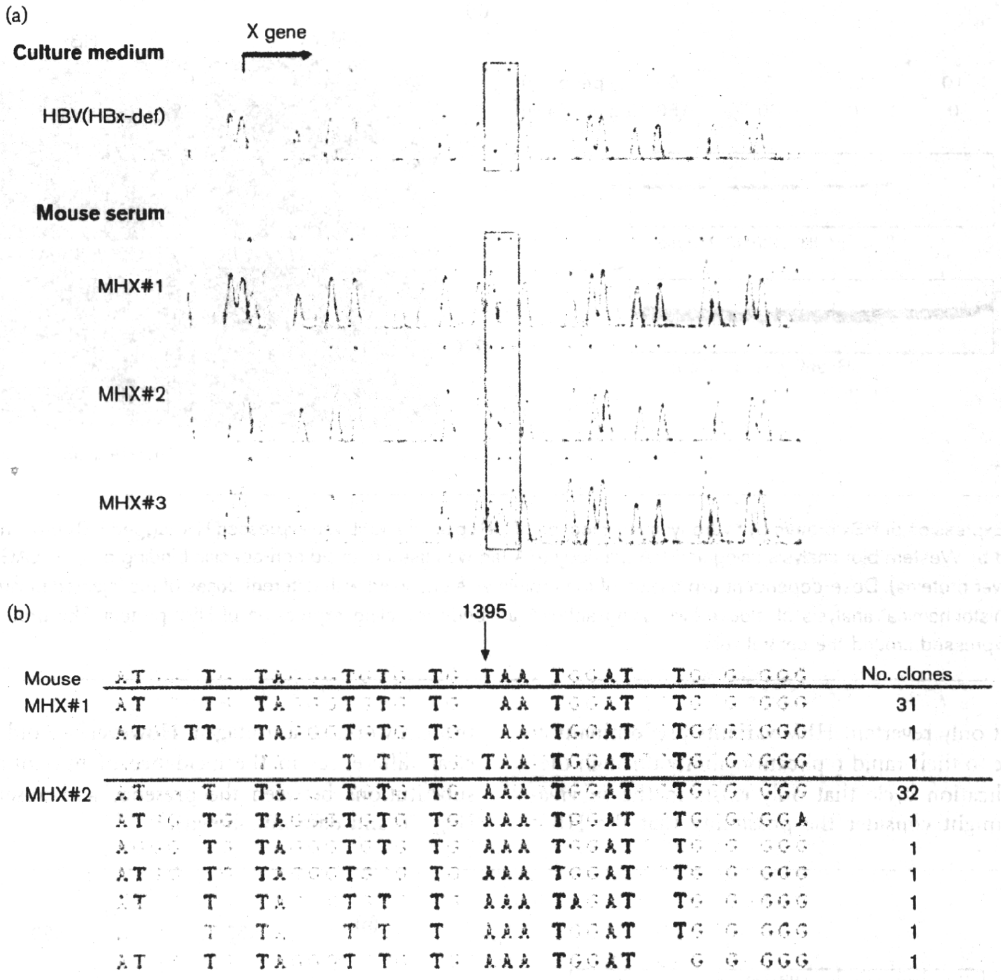

Fig. 7. Nucleotide sequence analysis of HBV recovered from HBx-def HBV-injected mice. (a) Nucleotide sequences of the HBx region of HBV determined by direct sequencing of PCR products using serum samples obtained from three mice (#1, #2 and #3 in Fig. 6a). The sequences were compared with that of inoculated HBV. Note that one of the three mice (#2) had a unique sequence different from the original sequence before introduction of the stop codon (C1395T). (b) Nucleotide sequences of the HBx gene determined by cloning and sequencing of PCR-amplified DNA from mice #1 and #2. Note that only one of 63 clones showed the introduced stop codon mutation. As we used a large amount of HBV plasmids, special care was taken to avoid contamination of DNA. Water was used as a negative control for all experiments and we observed no inappropriate amplification in these experiments.

It is thus still uncertain why the HBx protein is indispensable for virus replication *in vivo*. However, the fact that HBV cannot replicate in the absence of HBx protein may allow development of therapeutic medicine by disturbing the unknown action of HBx. To this end, it is interesting to identify a substance that binds to HBx.

The indispensability of the X protein for virus replication is a common feature shared by HBV and WHV (Chen *et al.*, 1993; Zoulim *et al.*, 1994). Both of them cause chronic infection, inflammation, fibrosis and cancer. In contrast, DHBV, which can replicate without DHBx expression, does not cause such a pathological situation (Meier *et al.*, 2003). Further analysis of the X protein may pave the way to clarify the mechanism of cancer development caused by HBV infection.

METHODS

Human hepatocyte chimeric mice experiments. Care of $uPA^{+/+}/SCID^{+/+}$ mice and transplantation of human hepatocytes were performed as described previously (Tateno *et al.*, 2004). The experiments were performed in accordance with the guidelines of the local committee for animal experiments at Hiroshima University. Infection, extraction of serum samples and sacrifice were performed under ether anaesthesia as described previously (Tateno *et al.*, 2004).

hAlb in mouse serum was measured with a Human Albumin ELISA Quantification kit (Bethyl Laboratories Inc.) according to the instructions provided by the manufacturer. Serum samples obtained from mice were aliquotted and stored in liquid nitrogen until use.

Analysis of HBV markers. HBsAg and HBeAg were measured using a commercially available ELISA kit (Abbott). For quantitative analysis of HBV DNA, 10 μl mouse serum sample or 100 μl of culture supernatant was used. DNA was extracted from these samples using the SMITEST R&D (Genome Science Laboratories) and dissolved in 20 μl H_2O, and HBV DNA was quantified by real-time PCR using the 7300 Real-Time PCR System (Applied Biosystems). Amplification was performed as described previously (Tsuge *et al.*, 2005). The lower detection limit of this assay is 300 copies. For detection of small amounts of HBV DNA, we also performed nested PCR. The amplification conditions were as described previously (Tsuge *et al.*, 2005).

Plasmid construction. The construction of wild-type (WT) HBV 1.4 genome length, pTRE-HB-wt, was described previously (Tsuge *et al.*, 2005). We used pTRE2 vector without pTet-off vector and doxycycline because a sufficient amount of HBV transcripts was produced from internal HBV promoters, and transcription from the pTRE2 promoter is negligible under these conditions. The nucleotide sequence of the HBV genome that we cloned into plasmid pTRE-HB-wt was deposited in GenBank under accession number AB206817. A modified plasmid, pTRE-HB-X-def, was generated by introducing a C-to-T point mutation at nt 1395 (aa 7) to create a stop codon (CAA to TAA) in the HBx gene (Fig. 1a). The substitution was introduced by using a QuikChange Site-Directed Mutagenesis kit (Stratagene). For the construction of the HBx gene expression plasmid, the HBx gene was amplified from pTRE-HB-wt and cloned into pcDNA3, pcDNA3-3 × HA, p3 × FLAG-CMV10 vectors and designated pcDNA-HBx, pcDNA3-HA-HBx, p3FLAG-HBx, respectively. Partially truncated HBx plasmids, with a deletion of the N-terminal 50 aa [HBx(51–154)] and the C-terminal 50 aa [HBx(1–50)], were also cloned into pcDNA3 or p3FLAG-CMV10 vectors.

Transfection of HepG2 cell lines with HBV expression plasmids. HepG2 cells were grown in Dulbecco's modified Eagle's medium supplemented with 10 % (v/v) fetal bovine serum at 37 °C and under 5 % CO_2. For functional analysis of the HBx protein *in vitro*, the HBV or HBx-def HBV expression plasmid was transfected with/without HBx expression plasmid using *Trans*IT-LT1 (Mirus) reagent according to the instructions provided by the supplier. Three to five days after transfection, core-associated HBV DNA was extracted from cells for HBV DNA quantification (Noguchi *et al.*, 2005). For analysing the infectivity of recombinant HBV particles, HBV expression plasmids were transiently transfected into HepG2 cells. The cells were seeded to semi-confluence in 90 mm dishes. WT HBV particles were generated from cells transfected with 20 μg pTRE2-HB-wt by calcium phosphate precipitation. HBx-def HBV particles were also generated from cells co-transfected with 10 μg pTRE2-HB-X-def and 10 μg pcDNA-HBx. Three days after transfection, the culture medium was collected and stored in liquid nitrogen until use.

Analysis of cell-culture-produced HBV by sucrose density gradient sedimentation. Five millilitres of HBV-positive human serum (8 $\log_{10}$ copies ml^{-1}) or 50 ml cell culture supernatant (8 $\log_{10}$ copies ml^{-1}) was layered on a 20 % (w/w) sucrose cushion, and centrifuged at 24 000 r.p.m. (maximum 103 864 *g*) for 12 h at 4 °C with a Beckman SW28 rotor (Beckman Coulter). The precipitate was resuspended in 500 μl PBS. These HBV samples were layered on a linear 20–50 % (w/w) sucrose gradient. Centrifugation was carried out at 24 000 r.p.m. (maximum 102 445 *g*) for 21 h at 4 °C with a Beckman SW40 rotor. The gradients were fractionated into 500 μl samples, and the density of each fraction was calculated from the weight and volume. Each fraction was diluted 10-fold and tested for HBV DNA by real-time PCR.

Analysis of replication intermediate of HBV. The cells were harvested 5 days after transfection and lysed with 250 μl lysis buffer [10 mM Tris/HCl (pH 7.4), 140 mM NaCl and 0.5 % (v/v) NP-40] followed by centrifugation for 2 min at 15 000 *g*. The core-associated HBV genome was immunoprecipitated by mouse anti-HBV core monoclonal antibody 2A21 (Institute of Immunology, Tokyo, Japan) and subjected to Southern blot analysis after SDS/proteinase K digestion, followed by phenol extraction and ethanol precipitation. Quantitative analysis was performed by real-time PCR with SYBR Green using the 7300 Real-Time PCR System and the amounts of the replication intermediates were compared. The HBV-specific primers used for amplification were 5′-TTTGGGCATGGACATTGAC-3′ and 5′-GGTGAACAATGTTCCGGAGAC-3′. The amplification conditions included initial denaturation at 95 °C for 10 min, followed by 45 cycles of denaturation at 95 °C for 15 s, annealing at 58 °C for 5 s and extension at 72 °C for 6 s. The lower detection limit of this assay was 300 copies.

Immunocytochemistry of HepG2 cells transfected with pTRE2-HB-X-def and p3FLAG-HBx plasmids. HepG2 cells were seeded to semi-confluence in two-well chamber plates. Each 1 μg pTRE2-HB-X-def and p3FLAG-HBx plasmids was co-transfected using *Trans*IT-LT1 reagent (Mirus) according to the instructions provided by the supplier. The cells were harvested 24 h after transfection and then washed with PBS and fixed with 4 % (v/v) paraformaldehyde. After fixation, the cells were stained with mouse monoclonal antibody directed to FLAG (Sigma) or rabbit polyclonal antibody against hepatitis B core antigen (HBcAg; DAKO Diagnostika) as the primary antibody. The bound antibodies were detected with an Alexa Fluor 488-conjugated antibody against rabbit IgG or Alexa Fluor 568-conjugated antibody against mouse IgG, respectively (Molecular Probes). Nuclei were counterstained with 6-diamidino-2-phenylindole (DAPI) (Vector Laboratories).

Hydrodynamic injection of HBx expression plasmids. Hydrodynamic injection was performed as reported previously (Yang *et al.*, 2002) with slight modifications. As the human hepatocyte chimeric mice were quite small (12–15 g) and weak for the rapid injection and the stress, we reduced the amount of DNA solution and injection speed: 1 ml PBS containing 30 μg HBx expression plasmids was injected rapidly through the mouse tail vein within 30 s. For analysis of infectivity of HBx-def HBV particles, the plasmids were injected twice a week.

Western blot analysis. Mouse liver tissues or transfected HepG2 cells were cooled on ice and treated with RIPA-like buffer [50 mM Tris/HCl (pH 8.0), 0.1 % SDS, 1 % NP-40, 150 mM sodium chloride and 0.5 % sodium deoxycholate] containing protease inhibitor cocktail (Sigma). Cell lysates were separated on SDS–polyacrylamide gels [5–20 % (w/v)] (Bio-Rad) and then transferred onto nitrocellulose membranes (GE Healthcare) by electroblotting. The membranes were incubated with anti-haemagglutinin fusion epitope (anti-HA) monoclonal antibody (Roche) or with anti β-actin monoclonal antibody (Sigma) followed by incubation with horseradish peroxidase-conjugated sheep anti-mouse immunoglobulin (GE Healthcare). Proteins were visualized via the ChemiDoc XRS system (Bio-Rad). Expression of HBc protein was quantified from the densities of the immunoblot signals by Quantity One software (Bio-Rad).

Immunohistochemical analysis of mouse liver. The liver specimens of HBV-infected mice were fixed with 10 % buffered paraformaldehyde and embedded in paraffin blocks for histological

examination. The liver sections were stained with haematoxylin–eosin or subjected to immunohistochemical staining using an antibody against HBcAg (DAKO Diagnostika), anti-HA antibody or HSA (Bethyl Laboratories Inc.). Endogenous peroxidase activity was blocked with 0.3 % H_2O_2 and methanol. Immunoreactive materials were visualized by using a streptavidin–biotin staining kit (Histofine SAB-PO kit; Nichirei) and diaminobenzidine.

Sequence analysis of the HBV genome. Genome-length HBV DNA was amplified by PCR as described by Günther *et al.* (1995). HBV genome-length PCR products were subjected to 1 % agarose gel electrophoresis and the 3.2 kbp band was extracted using a QiaEx II Gel Extraction kit (Qiagen). Direct sequencing, cloning and sequencing (Ohishi *et al.*, 2004) were performed in an ABI PRISM 3100-Avant Genetic Analyzer (Applied Biosystems) with a Big Dye Terminator version 3.0 Cycle Sequencing Ready Reaction kit (Applied Biosystems).

Statistical analysis. All data are expressed as mean ± SD. Differences between groups were examined for statistical significance by using Student's *t*-test. A P value <0.05 denoted the presence of a statistically significant difference.

ACKNOWLEDGEMENTS

This work was carried out at the Research Center for Molecular Medicine, Faculty of Medicine, Hiroshima University, and the Analysis Center of Life Science, Hiroshima University. The authors thank Chiemi Noguchi and Waka Ohishi for their helpful discussion, Kana Kunihiro for her excellent technical assistance, and Yoshiko Nakata and Aya Furukawa for secretarial assistance. Financial support was provided by the Ministry of Education, Sports, Culture and Technology and Ministry of Health, Labour and Welfare (Grants-in-Aid for scientific research and development).

REFERENCES

Ando, T., Sugiyama, K., Goto, K., Miyake, Y., Li, R., Kawabe, Y. & Wada, Y. (1999). Age at time of hepatitis Be antibody seroconversion in childhood chronic hepatitis B infection and mutant viral strain detection rates. *J Pediatr Gastroenterol Nutr* **29**, 583–587.

Arbuthnot, P., Capovilla, A. & Kew, M. (2000). Putative role of hepatitis B virus X protein in hepatocarcinogenesis: effects on apoptosis, DNA repair, mitogen-activated protein kinase and JAK/STAT pathways. *J Gastroenterol Hepatol* **15**, 357–368.

Bouchard, M. J., Wang, L. H. & Schneider, R. J. (2001). Calcium signaling by HBx protein in hepatitis B virus DNA replication. *Science* **294**, 2376–2378.

Chen, H. S., Kaneko, S., Girones, R., Anderson, R. W., Hornbuckle, W. E., Tennant, B. C., Cote, P. J., Gerin, J. L., Purcell, R. H. & Miller, R. H. (1993). The woodchuck hepatitis virus X gene is important for establishment of virus infection in woodchucks. *J Virol* **67**, 1218–1226.

Colgrove, R., Simon, G. & Ganem, D. (1989). Transcriptional activation of homologous and heterologous genes by the hepatitis B virus X gene product in cells permissive for viral replication. *J Virol* **63**, 4019–4026.

Dandri, M., Schirmacher, P. & Rogler, C. E. (1996). Woodchuck hepatitis virus X protein is present in chronically infected woodchuck liver and woodchuck hepatocellular carcinomas which are permissive for viral replication. *J Virol* **70**, 5246–5254.

Dandri, M., Petersen, J., Stockert, R. J., Harris, T. M. & Rogler, C. E. (1998). Metabolic labeling of woodchuck hepatitis B virus X protein in naturally infected hepatocytes reveals a bimodal half-life and association with the nuclear framework. *J Virol* **72**, 9359–9364.

Doria, M., Klein, N., Lucito, R. & Schneider, R. J. (1995). The hepatitis B virus HBx protein is a dual specificity cytoplasmic activator of Ras and nuclear activator of transcription factors. *EMBO J* **14**, 4747–4757.

Ganem, D. & Schneider, R. J. (2001). *Hepadnaviridae*: the viruses and their replication. In *Fields Virology*, 4th edn, pp. 2923–2969. Edited by D. M. Knipe, P. M. Howley, D. E. Griffin, R. A. Lamb, M. A. Martin, B. Roizman & S. E. Straus. Philadelphia, PA: Lippincott Williams & Wilkins.

Günther, S., Li, B. C., Miska, S., Kruger, D. H., Meisel, H. & Will, H. (1995). A novel method for efficient amplification of whole hepatitis B virus genomes permits rapid functional analysis and reveals deletion mutants in immunosuppressed patients. *J Virol* **69**, 5437–5444.

Henkler, F., Hoare, J., Waseem, N., Goldin, R. D., McGarvey, M. J., Koshy, R. & King, I. A. (2001). Intracellular localization of the hepatitis B virus HBx protein. *J Gen Virol* **82**, 871–882.

Jacob, J. R., Ascenzi, M. A., Roneker, C. A., Toshkov, I. A., Cote, P. J., Gerin, J. L. & Tennant, B. C. (1997). Hepatic expression of the woodchuck hepatitis virus X-antigen during acute and chronic infection and detection of a woodchuck hepatitis virus X-antigen antibody response. *Hepatology* **26**, 1607–1615.

Keasler, V. V., Hodgson, A. J., Madden, C. R. & Slagle, B. L. (2007). Enhancement of hepatitis B virus replication by the regulatory X protein *in vitro* and *in vivo*. *J Virol* **81**, 2656–2662.

Klein, N. P., Bouchard, M. J., Wang, L. H., Kobarg, C. & Schneider, R. J. (1999). Src kinases involved in hepatitis B virus replication. *EMBO J* **18**, 5019–5027.

Leupin, O., Bontron, S., Schaeffer, C. & Strubin, M. (2005). Hepatitis B virus X protein stimulates viral genome replication via a DDB1-dependent pathway distinct from that leading to cell death. *J Virol* **79**, 4238–4245.

Meier, P., Scougall, C. A., Will, H., Burrell, C. J. & Jilbert, A. R. (2003). A duck hepatitis B virus strain with a knockout mutation in the putative X ORF shows similar infectivity and *in vivo* growth characteristics to wild-type virus. *Virology* **317**, 291–298.

Melegari, M., Wolf, S. K. & Schneider, R. J. (2005). Hepatitis B virus DNA replication is coordinated by core protein serine phosphorylation and HBx expression. *J Virol* **79**, 9810–9820.

Mercer, D. F., Schiller, D. E., Elliott, J. F., Douglas, D. N., Hao, C., Rinfret, A., Addison, W. R., Fischer, K. P., Churchill, T. A. & other authors (2001). Hepatitis C virus replication in mice with chimeric human livers. *Nat Med* **7**, 927–933.

Murakami, S. (2001). Hepatitis B virus X protein: a multifunctional viral regulator. *J Gastroenterol* **36**, 651–660.

Noguchi, C., Ishino, H., Tsuge, M., Fujimoto, Y., Imamura, M., Takahashi, S. & Chayama, K. (2005). G to A hypermutation of hepatitis B virus. *Hepatology* **41**, 626–633.

Ohishi, W., Shirakawa, H., Kawakami, Y., Kimura, S., Kamiyasu, M., Tazuma, S., Nakanishi, T. & Chayama, K. (2004). Identification of rare polymerase variants of hepatitis B virus using a two-stage PCR with peptide nucleic acid clamping. *J Med Virol* **72**, 558–565.

Raney, A. K. & McLachlan, A. (1991). The biology of hepatitis B virus. In *Molecular Biology of the Hepatitis B Virus*, pp. 1–37. Edited by A. McLachlan. Boca Raton, FL: CRC Press.

Seeger, C. & Mason, W. S. (2000). Hepatitis B virus biology. *Microbiol Mol Biol Rev* **64**, 51–68.

Sitterlin, D., Bergametti, F., Tiollais, P., Tennant, B. C. & Transy, C. (2000a). Correct binding of viral X protein to UVDDB-p127 cellular protein is critical for efficient infection by hepatitis B viruses. *Oncogene* **19**, 4427–4431.

Sitterlin, D., Bergametti, F. & Transy, C. (2000b). UVDDB p127-binding modulates activities and intracellular distribution of hepatitis B virus X protein. *Oncogene* **19**, 4417–4426.

Su, Q., Schroder, C. H., Hofmann, W. J., Otto, G., Pichlmayr, R. & Bannasch, P. (1998). Expression of hepatitis B virus X protein in HBV-infected human livers and hepatocellular carcinomas. *Hepatology* 27, 1109–1120.

Tang, H., Banks, K. E., Anderson, A. L. & McLachlan, A. (2001). Hepatitis B virus transcription and replication. *Drug News Perspect* **14**, 325–334.

Tang, H., Delgermaa, L., Huang, F., Oishi, N., Liu, L., He, F., Zhao, L. & Murakami, S. (2005). The transcriptional transactivation function of HBx protein is important for its augmentation role in hepatitis B virus replication. *J Virol* **79**, 5548–5556.

Tateno, C., Yoshizane, Y., Saito, N., Kataoka, M., Utoh, R., Yamasaki, C., Tachibana, A., Soeno, Y., Asahina, K. & other authors (2004). Near completely humanized liver in mice shows human-type metabolic responses to drugs. *Am J Pathol* **165**, 901–912.

Tsuge, M., Hiraga, N., Takaishi, H., Noguchi, C., Oga, H., Imamura, M., Takahashi, S., Iwao, E., Fujimoto, Y. & other authors (2005). Infection of human hepatocyte chimeric mouse with genetically engineered hepatitis B virus. *Hepatology* **42**, 1046–1054.

Wang, W. L., London, W. T. & Feitelson, M. A. (1991). Hepatitis B X antigen in hepatitis B virus carrier patients with liver cancer. *Cancer Res* **51**, 4971–4977.

Xu, Z., Yen, T. S., Wu, L., Madden, C. R., Tan, W., Slagle, B. L. & Ou, J. H. (2002). Enhancement of hepatitis B virus replication by its X protein in transgenic mice. *J Virol* **76**, 2579–2584.

Yang, P. L., Althage, A., Chung, J. & Chisari, F. V. (2002). Hydrodynamic injection of viral DNA: a mouse model of acute hepatitis B virus infection. *Proc Natl Acad Sci U S A* **99**, 13825–13830.

Zhang, Z., Torii, N., Hu, Z., Jacob, J. & Liang, T. J. (2001). X-deficient woodchuck hepatitis virus mutants behave like attenuated viruses and induce protective immunity *in vivo*. *J Clin Invest* **108**, 1523–1531.

Zoulim, F., Saputelli, J. & Seeger, C. (1994). Woodchuck hepatitis virus X protein is required for viral infection *in vivo*. *J Virol* **68**, 2026–2030.

Journal of General Virology (2010), 91, 1668–1677 DOI 10.1099/vir.0.019315-0

Practical evaluation of a mouse with chimeric human liver model for hepatitis C virus infection using an NS3-4A protease inhibitor

Naohiro Kamiya,[1] Eiji Iwao,[1] Nobuhiko Hiraga,[2,3] Masataka Tsuge,[2,3] Michio Imamura,[2,3] Shoichi Takahashi,[2,3] Shinji Miyoshi,[4] Chise Tateno,[3,5] Katsutoshi Yoshizato[3,5] and Kazuaki Chayama[2,3]

Correspondence
Kazuaki Chayama
chayama@hiroshima-u.ac.jp

[1]Pharmacology Department V, Mitsubishi Tanabe Pharma Corporation, Yokohama, Japan

[2]Department of Medicine and Molecular Science, Division of Frontier Medical Science, Programs for Biomedical Research, Graduate School of Biomedical Sciences, Hiroshima University, Hiroshima, Japan

[3]Liver Research Project Center, Hiroshima University, Hiroshima, Japan

[4]DMPK Department, Mitsubishi Tanabe Pharma Corporation, Kisarazu, Chiba, Japan

[5]PhoenixBio, Higashihiroshima, Japan

A small-animal model for hepatitis C virus (HCV) infection was developed using severe combined immunodeficiency (SCID) mice encoding homozygous urokinase-type plasminogen activator (uPA) transplanted with human hepatocytes. Currently, limited information is available concerning the HCV clearance rate in the SCID mouse model and the virion production rate in engrafted hepatocytes. In this study, several cohorts of $uPA^{+/+}/SCID^{+/+}$ mice with nearly half of their livers repopulated by human hepatocytes were infected with HCV genotype 1b and used to evaluate HCV dynamics by pharmacokinetic and pharmacodynamic analyses of a specific NS3-4A protease inhibitor (telaprevir). A dose-dependent reduction in serum HCV RNA was observed. At telaprevir exposure equivalent to that in clinical studies, rapid turnover of serum HCV was also observed in this mouse model and the estimated slopes of virus decline were 0.11–0.17 $\log_{10}$ h^{-1}. During the initial phase of treatment, the $\log_{10}$ reduction level of HCV RNA was dependent on the drug concentration, which was about fourfold higher in the liver than in plasma. HCV RNA levels in the liver relative to human endogenous gene expression were correlated with serum HCV RNA levels at the end of treatment for up to 10 days. A mathematical model analysis of viral kinetics suggested that 1 g of the chimeric human liver could produce at least 10^8 virions per day, and this may be comparable to HCV production in the human liver.

Received 17 December 2009
Accepted 17 February 2010

INTRODUCTION

Hepatitis C virus (HCV) is a major cause for concern worldwide. More than 3 % of the world's population is chronically infected with HCV and 3–4 million people are newly infected each year (Wasley & Alter, 2000). Chronic HCV infection is relatively mild and progresses slowly; however, about 20 % of chronic hepatitis C (CHC) carriers progress to serious end-stage liver disease (Lauer & Walker, 2001; Liang *et al.*, 2000; Poynard *et al.*, 2003). The current standard treatment for HCV infection is administration of pegylated alpha interferon (PEG-IFN) in combination with ribavirin (RBV) for 48 weeks. The overall cure rates with this intervention are 40–50 % for patients with genotype 1 and more than 75 % for patients with genotypes 2 and 3 (Fried *et al.*, 2002; Manns *et al.*, 2001). Several compounds that inhibit specific stages of the virus life cycle have been clinically evaluated (Manns *et al.*, 2007; Pereira & Jacobson, 2009). Telaprevir is a novel peptidomimetic slow- and tight-binding inhibitor of HCV NS3-4A protease, which was discovered using a structure-based drug design approach (Perni *et al.*, 2006). A rapid decline in viral RNA was observed in CHC patients treated with telaprevir (Reesink *et al.*, 2006) and an increased antiviral effect of a combination of telaprevir and PEG-IFN has been reported (Forestier *et al.*, 2007). Recent clinical trials of telaprevir in combination with PEG-IFN and RBV have indicated a promising material advance in therapy for CHC patients (Hézode *et al.*, 2009; McHutchison *et al.*, 2009). First-generation HCV-specific agents have been developed despite the lack of small-animal models for HCV infection. However, early emergence of resistant variants against novel antiviral agents is a concern. Thus, the use of two or more investigation agents is strongly recommended for

019315 © 2010 SGM *Printed in Great Britain*

clinical studies in CHC patients (Sherman *et al.*, 2007). To ensure ethical and safe clinical trials, animal models continue to be necessary for the mechanistic evaluation of the ability of specific agents to inhibit the virus life cycle *in vivo* and to develop better therapeutic strategies, including combination regimens (Boonstra *et al.*, 2009). Several groups have developed a small-animal model for HCV infection using homozygous urokinase-type plasminogen activator (uPA)/severe combined immunodeficiency (SCID) ($uPA^{+/+}/SCID^{+/+}$) mice transplanted with human hepatocytes (Mercer *et al.*, 2001). These mice are susceptible to cell culture-grown HCV (HCVcc; Lindenbach *et al.*, 2006) and have been used to evaluate antiviral agents including IFN-α, BILN 2061 (an NS3-4A protease inhibitor) and HCV796 (an NS5B polymerase inhibitor) (Kneteman *et al.*, 2006, 2009; Vanwolleghem *et al.*, 2007). However, the HCV clearance rate in the SCID mouse model and the virion production rate in hepatocytes engrafted in the mouse liver are not fully understood. We also generated a mouse model with an almost humanized liver (Tateno *et al.*, 2004). Using this mouse model, we reported the infection of a genetically engineered hepatitis B virus (Tsuge *et al.*, 2005) and developed a reverse genetics system for HCV genotypes 1a, 1b and 2a after intrahepatic injection of *in vitro*-transcribed RNA as well as intravenous injection of HCVcc (Hiraga *et al.*, 2007; Kimura *et al.*, 2008). In this study, we demonstrated the rapid turnover of serum HCV RNA and the pharmacokinetics (PK) and pharmacodynamics (PD) of telaprevir treatment. We concluded after quantitative estimation and the use of a mathematical model that HCV production equivalent to that in the human liver is possible in engrafted hepatocytes in this mouse model.

RESULTS

Preliminary dose-finding study

At the beginning of this study, we attempted to determine an effective dose regimen for telaprevir in this mouse model. Nine mice were randomized and treated with telaprevir over three time periods (Table 1). The lifetime kinetics of serum HCV RNA and of human serum albumin (HSA) in blood are represented in Fig. 1. One mouse (A07) exhibited a rapid reduction in HSA in the blood, which indicated the instability of human hepatocyte grafts. As a rapid reduction in HSA levels was not observed in subsequent experiments, this mouse was excluded from the mean analysis. After 7 days of twice daily (BID) dosing in period 1, the mean $\log_{10}$ changes in HCV RNA from baseline ($\pm$SEM) after the 100 and 10 mg telaprevir kg^{-1} doses were -0.49 ± 0.094 and -0.53 ± 0.039, respectively, and no dose-dependent reduction was observed. During period 2, the dose frequency was changed from BID to three times daily (TID), and the time of serum sampling was also changed from 1 to 4 h after the last dose. After the 3-day treatment, the mean $\log_{10}$ changes of HCV RNA in 100 and 10 mg telaprevir kg^{-1} TID groups were -1.00 ± 0.166 and -0.28 ± 0.056, respectively, and the difference between the two groups was significant. To test the reproducibility of results, mice were treated with 10 or 100 mg telaprevir kg^{-1} TID for 10 days and then sacrificed 5 h after the administration of the last dose. The mean $\log_{10}$ changes in serum HCV RNA were -1.46 ± 0.265 and -0.27 ± 0.073 in the 100 and 10 mg kg^{-1} TID groups, respectively, and the difference between the means was significant.

Evaluation of HCV turnover in this mouse model

Because of the SCID nature of this mouse model, the virion clearance mechanism was of interest. Six mice with steady-state and high viral loads (9.7×10^5–1.2×10^8 copies ml^{-1}) were administered 200 mg telaprevir kg^{-1} TID for 4 days, with 5 h intervals between doses and a 14 h intermission from drug treatment each day. Because the $\log_{10}$ reduction in HCV RNA appeared to depend on the time of serum collection during the day (Fig. 2a), the mean $\log_{10}$ changes in HCV RNA were plotted against time and fitted to a linear regression model (Fig. 2b). The estimated slopes (i.e. $\log_{10}$ HCV reduction per hour) and 95% confidence intervals (CI) on days 1, 2 and 3 were -0.165 (-0.268 to 0.0616), -0.115 (-0.131 to 0.0990) and -0.153, respectively. These regression lines also suggested that extrapolated HCV loads at the actual times of the daily first doses were 0.0530, -0.220 and -0.0948 $\log_{10}$ copies ml^{-1}, respectively. Therefore, it appeared that the viral load

Table 1. Telaprevir dose-finding experiment

Period	Duration (days)	Frequency of dose (per day)	Dose (mg kg^{-1})	No. of mice	Mean $\log_{10}$ changes ± SEM	*P* value (*t* test)
1	7	2	100	4	-0.49 ± 0.094	0.7806
			10	3*	-0.53 ± 0.039	
			0	1	-0.47	
2	3	3	100	4*	-1.00 ± 0.166	0.0064
			10	4	-0.28 ± 0.056	
3	10	3	100	3	-1.46 ± 0.265	0.0125
			10	3	-0.27 ± 0.073	

*One mouse was excluded because of instability of human hepatocyte grafts.

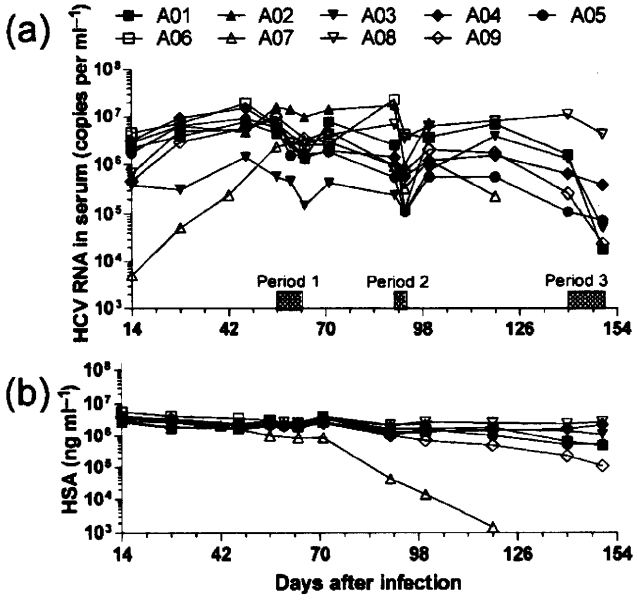

Fig. 1. Lifelong changes in serum HCV RNA and HSA in the blood of HCV-infected mice in the preliminary dose-finding experiment. Nine HCV-infected mice (A01–A09) were treated with telaprevir over three independent periods. The mice were treated with 10 mg telaprevir kg^{-1}, 100 mg telaprevir kg^{-1} or vehicle BID for 7 days (period 1), TID for 3 days (period 2) and TID for 10 days (period 3). (a) Kinetics of serum HCV RNA. (b) Kinetics of HSA level in blood. Because the HSA level indicated the stability of engrafted human hepatocytes in the mice, mouse A07 was excluded from the summary of the results in Table 1.

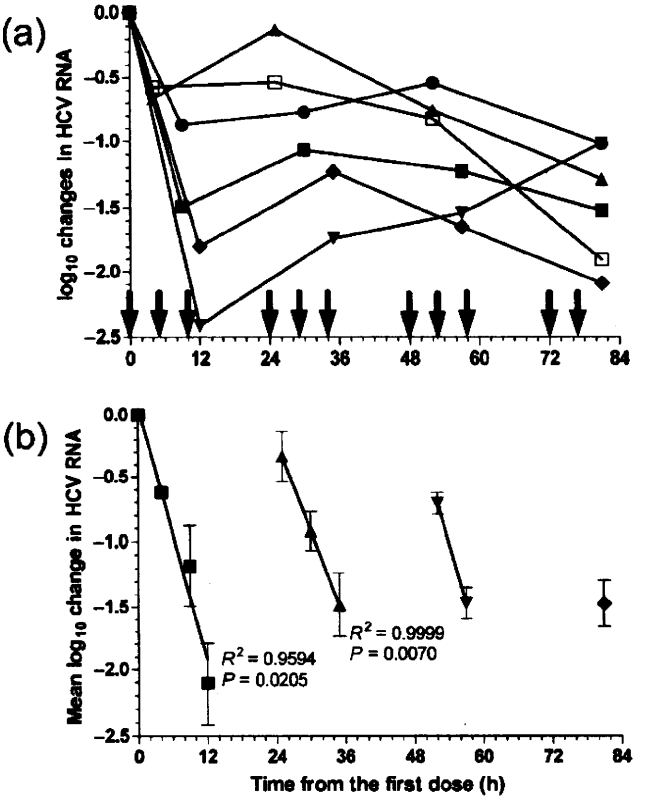

Fig. 2. Estimation of virus clearance rate. Six HCV-infected mice were treated with 200 mg telaprevir kg^{-1} TID for 4 days. Individual kinetics of $\log_{10}$ reductions in serum HCV RNA (a) and of mean $\log_{10}$ changes (± SEM) at each sampling time (b) are represented. Arrows indicate the times of dosing. The slopes of mean $\log_{10}$ HCV RNA reduction were estimated by linear regression analysis. P and R^2 values are indicated on the figure.

reverted back towards baseline levels during the 14 h intermission from drug treatment.

PK analysis

To assess drug exposure after repeated dosing in this mouse model, mice were administered 100 or 300 mg telaprevir kg^{-1} BID for 4 days. The mice receiving 300 mg kg^{-1} BID for 4 days had a mean 2 $\log_{10}$-fold HCV reduction, whereas those receiving 100 mg kg^{-1} BID had up to a 1.5 $\log_{10}$-fold reduction by day 3 (Fig. 3a). Plasma telaprevir concentrations after administration of the final dose are indicated in Fig. 3(b). The estimated half-life of telaprevir in the 100 and 300 mg kg^{-1} groups was 2.4 and 3.8 h, respectively.

PK/PD analysis and the dose-dependent reduction in HCV RNA

To evaluate the correlation between telaprevir concentration and HCV reductions in this mouse model, we used another cohort of 12 HCV-infected mice with high viral loads (1.6×10^6–3.9×10^8 copies ml^{-1}). In this crossover study, mice were randomized into three groups (n=4 each), each of which underwent two periods of dosing for 5 days separated by a 1-week washout period. Serum and plasma samples were collected once daily 5 h after dosing. The mean $\log_{10}$ changes in HCV RNA (± SEM) at different dose levels were calculated from the combined results of both periods (Fig. 4a). The mean $\log_{10}$ reductions from baseline in the 100 and 300 mg kg^{-1} groups were approximately 1 $\log_{10}$ and 1.5–2 $\log_{10}$, respectively, and the difference between the two groups was statistically significant. The means calculated in each period separately are also shown in Fig. 4(b). The plasma telaprevir concentration was positively correlated with the $\log_{10}$ HCV RNA reduction level in each period (Fig. 4c).

Drug concentrations and HCV levels in blood correlate with those in the liver

The correlation between telaprevir concentrations in the plasma and liver was analysed in a double logarithmic plot 5 (dose-finding cohort) or 8 h (PK and PK/PD cohorts) after the last dose (Fig. 5). The linear regression lines suggested that telaprevir concentrations in the liver were 5–

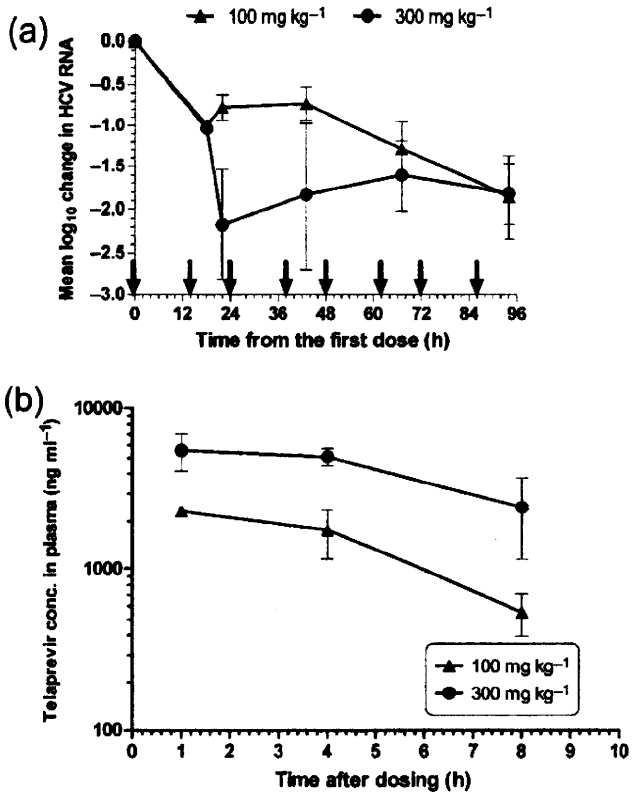

Fig. 3. PK analysis of telaprevir in the HCV-infected mouse model. Six HCV-infected mice were administered 100 (n=3) or 300 (n=3) mg telaprevir kg^{-1} BID for 4 days and serum samples were collected once daily to assess antiviral activity. After the last dose, plasma samples were collected at 1, 4 and 8 h for PK analysis. (a) Mean $\log_{10}$ changes (± SEM) in serum HCV RNA from mice treated with telaprevir. Arrows indicate the times of dosing. (b) Kinetics of telaprevir concentrations in plasma after the last dose.

10-fold higher at 5 h and approximately fourfold higher at 8 h than those in plasma. Total cellular RNA samples were extracted from two, one and four discrete small sections (approx. 50 mg) of the liver in the preliminary dose-finding, PK and PK/PD cohorts, respectively. HCV RNA levels in the total cellular RNA extract were relatively quantified by duplex real-time RT-PCR analysis using human β_2-microglobulin (hβ_2m) as an internal standard of human endogenous gene expression. Neither the threshold cycle (Ct) of hβ_2m ($Ct_{h\beta 2m}$) nor the Ct of HCV (Ct_{HCV}) correlated with total RNA from a small section of the chimeric human livers (data not shown). This result indicated that occupancy rates of human cells varied individually and/or among small sections of the chimeric human liver. Therefore, the mean difference in Ct ($\Delta Ct = Ct_{HCV} - Ct_{h\beta 2m}$) in each mouse was calculated and plotted against the viral load in serum (Fig. 6). After treatment with telaprevir for up to 10 days, mean ΔCt values ranged between 11 (HCV RNA content: $2^{11} = 2 \times 10^3$-fold lower than hβ_2m expression) and 17 (1×10^5-fold lower) among the HCV-infected mice and correlated linearly with $\log_{10}$ serum HCV RNA levels.

Viral dynamics model analysis

To evaluate time-dependent reductions in HCV with BID dosing, 12 HCV-infected elderly mice, which maintained high and steady-state viral loads (1.2×10^6–8.5×10^7 copies ml^{-1}) for more than 6 months, were treated with 200 mg telaprevir kg^{-1} BID for 3 days. The mice were divided into two groups, and serum samples were collected just before the second dose and 4 (n=6) or 8 (n=6) h after every two administrations. The single administration of telaprevir resulted in a mean 0.8–1.0 $\log_{10}$-fold reduction in HCV RNA in both groups. After the second dose, the pattern of viral kinetics appeared to depend on the time of serum collection, and the mean HCV RNA reduction level was higher in the 8 h group than in the 4 h group and plateaued at approximately a 2 $\log_{10}$-fold reduction in both groups after treatment for 3 days (Fig. 7). Finally, we attempted to estimate parameters of efficacy (ε) and virus clearance (c) per hour in this mouse model for comparison with estimates derived from human studies. Because the mean viral kinetics of the 8 h group was biphasic, the values in the 8 h group were used together for the mathematical model analysis. The estimated ε and c values were 0.992 (95 % CI 0.982–1.00) and 0.200 (95 % CI 0.110–0.291), respectively.

DISCUSSION

Using a mouse model with a chimeric human liver for HCV infection, we analysed the PK/PD of telaprevir treatment and investigated HCV dynamics during the initial phase of protease inhibitor treatment. All the mice in this study were expected to have more than half of their livers repopulated by human hepatocytes (Tateno *et al.*, 2004), which simulates a human drug metabolism profile (Katoh *et al.*, 2007, 2008). After the infection with HCV genotype 1b, high viral loads were maintained in the mice for more than 6 months. Recent studies have indicated the utility of a human/mouse chimera model for HCV infection to evaluate antiviral efficacy (Kneteman *et al.*, 2006, 2009) and preclinical safety (Vanwolleghem *et al.*, 2007). However, PK/PD studies and estimations of virus clearance rate have rarely been performed in this mouse model. HCV production, including intracellular replication in engrafted hepatocytes, has also not yet been elucidated. Despite the SCID nature of this mouse model, a 2 $\log_{10}$-fold HCV RNA reduction was observed within 0.5 days, as has been observed previously in CHC patients (Forestier *et al.*, 2007; Reesink *et al.*, 2006). In this mouse model, the rapid rebound in HCV load during the intermission from drug exposure indicated the rapid production and release of HCV into the circulation. This finding indicates that a virion-clearing compartment, which does not depend on T- and B-cell responses, may exist in this mouse model.

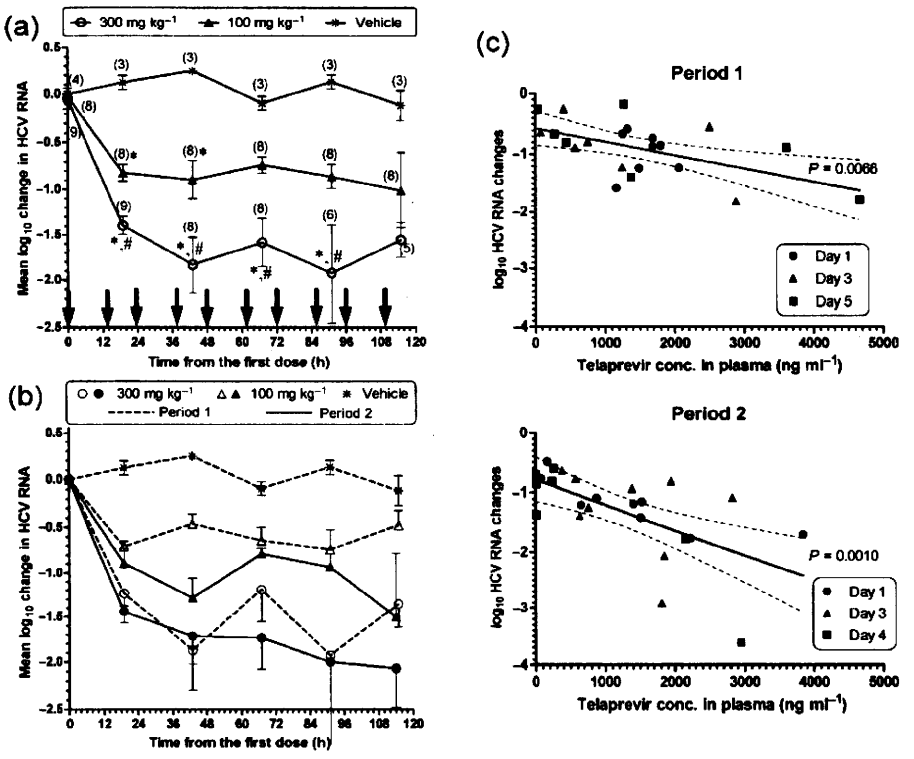

Fig. 4. PK/PD analysis and the dose-dependent reduction in HCV. Twelve HCV-infected mice were randomized into three groups (n=4 each) and then underwent two periods of telaprevir BID dosing for 5 days, separated by a 1-week washout period. Before the second period, the mice in the vehicle control group were additionally assigned to active drug groups. During the second period, mice that received the high or low doses were crossed over to the alternative treatment. Serum and plasma samples were collected once daily 5 h after dosing. Mean $\log_{10}$ changes (± SEM) in serum HCV RNA were calculated from the combined results from both periods (a) and each period separately (b). Arrows indicate the times of dosing. *, $P<0.05$ versus vehicle control group; #, $P<0.05$ versus 100 mg kg^{-1} group. (c) Correlation between $\log_{10}$ reduction in serum HCV and telaprevir concentrations in plasma. Linear regressions (solid lines) and 95 % CI (dashed lines) are indicated.

One possible explanation is that viral kinetics after liver transplantation in humans may play a role in HCV clearance under immunosuppressed conditions (Dahari *et al.*, 2005; Powers *et al.*, 2006; Schiano *et al.*, 2005). This observation suggests that this mouse model is capable of evaluating 'first-phase' HCV clearance after drug treatment.

In a clinical trial of telaprevir, CHC patients who exhibited a continuous decline in viral kinetics had mean plasma trough levels above 1000 ng ml^{-1}; therefore, a dose of 750 mg TID was selected for further clinical studies (Sarrazin *et al.*, 2007). When HCV-infected mice were administered 100 or 300 mg telaprevir kg^{-1}, a plasma concentration above 1000 ng ml^{-1} was maintained beyond 8 h in mice treated with 300 mg kg^{-1} but not in those treated with 100 mg kg^{-1}. This result suggests that the extrapolation of telaprevir doses from this mouse model to human studies depends on body surface area, i.e. approximately 15th of a dose in this mouse model may be equivalent to a dose in humans. In another cohort of mice treated with 100 and 300 mg telaprevir kg^{-1} BID, a dose-dependent reduction in HCV was observed and the plasma telaprevir concentration correlated significantly with the HCV reduction level. Therefore, the PK/PD results in this mouse model may be able to indicate a targeted dose range in clinical studies.

Whereas a telaprevir concentration in plasma equivalent to its dosage in clinical trials was achieved in this mouse model, the serum HCV RNA level plateaued at a decrease of approximately 2 $\log_{10}$-fold within several days of treatment. A saturated reduction of approximately 2 $\log_{10}$-fold after treatments with BILN 2061 and IFN was also reported in an analogous mouse model (Kneteman *et al.*, 2006; Vanwolleghem *et al.*, 2007). These observations led us to examine HCV replication in the chimeric human liver. In the relative quantification of HCV RNA against human-specific endogenous gene expression, we observed a correlation between the serum HCV RNA level and the mean ΔCt value in the liver, despite no correlation between the total RNA concentration and each Ct value of two target genes in the liver RNA extracts. This result can be interpreted to indicate that HCV replicated only in

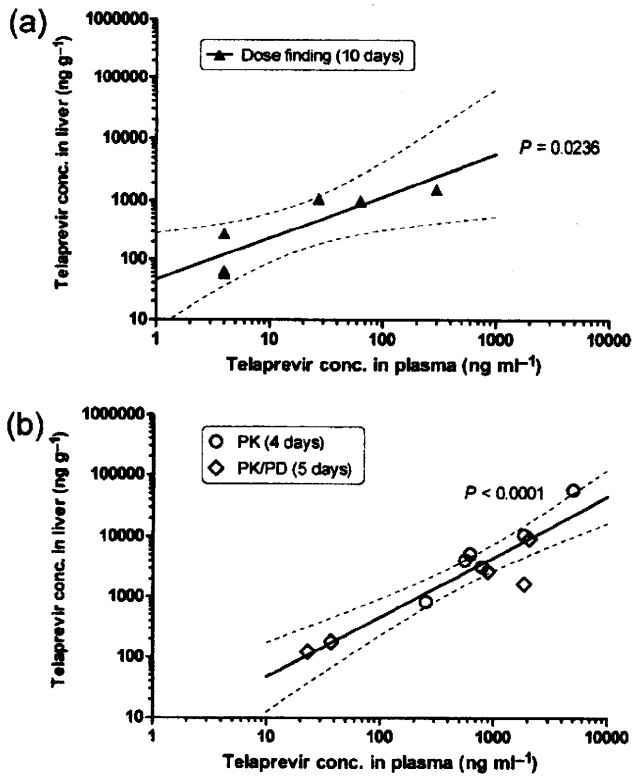

Fig. 5. Correlation between telaprevir concentrations in the liver and plasma. Telaprevir concentrations in the liver and plasma were determined at the end of the three different experiments indicated in Fig. 1 (dose-finding), Fig. 3 (PK) and Fig. 4 (PK/PD). Telaprevir concentrations in the liver were plotted against those in plasma 5 (a) or 8 (b) h after the last dose. Linear regressions (solid lines) and 95 % CI (dashed lines) are indicated.

engrafted human hepatocytes, and the observed HCV reduction in serum might reflect virus replication in the human hepatocyte grafts. Moreover, the relative content of HCV RNA was 2×10^3–1×10^5-fold lower than hβ_2m expression, whereas an HCV replicon cell line, which had approximately 1000 replicon genomes per cell (Quinkert *et al.*, 2005), contained nearly equal amounts of both genes (data not shown). HCV replication was much lower in the engrafted human hepatocytes than in an HCV replicon cell line, and HCV infected only a small portion of the engrafted human hepatocytes. It has been reported that 4–25 % of hepatocytes in a CHC patient were positive for replicative-intermediate RNA, and the mean number of viral genomes per productively infected hepatocyte ranged from 7 to 64 molecules (Chang *et al.*, 2003). Also, a more recent report suggested that the percentage of HCV antigen-positive hepatocytes in patients varied from 0 to 40 %, and the HCV content in 2000 microdissected HCV-positive cells ranged from 40 to 1800 international units using a branched DNA assay (Vona *et al.*, 2004). Therefore, we suggest that HCV replication efficiency in engrafted human hepatocytes is equivalent to that in CHC patients.

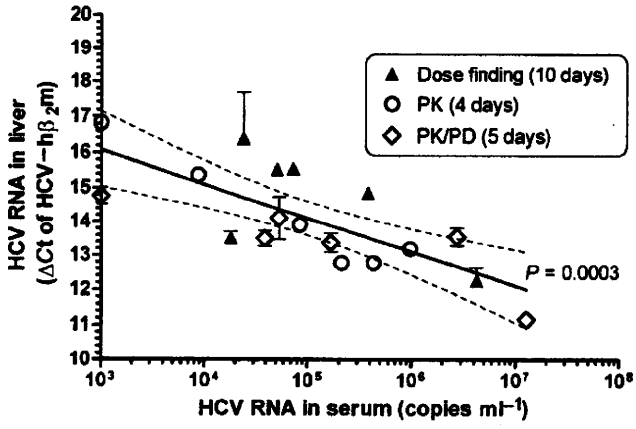

Fig. 6. Correlation between HCV content in the liver and serum. Relative quantification of HCV RNA levels in the liver was determined by the difference between threshold cycles (ΔCt) of HCV RNA and hβ_2m in a duplex real-time RT-PCR analysis. Linear regressions (solid line) and 95 % CI (dashed lines) are indicated.

The differences observed between the engrafted human hepatocytes and the HCV replicon cell line can be explained by the following assumptions: approximately 10 % of engrafted human hepatocytes are productively

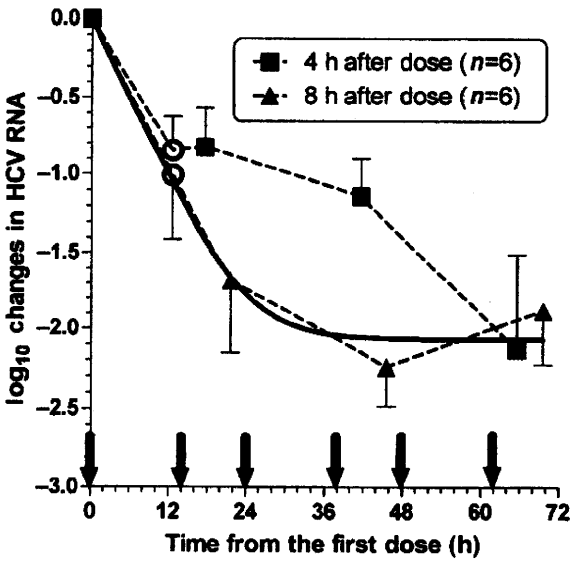

Fig. 7. Viral dynamics under BID telaprevir treatment. Mice were administered 200 mg telaprevir kg^{-1} BID at the times indicated by arrows. Serum samples were collected just before the second dose was administered and 4 (n=6) or 8 (n=6) h after every two doses were administered. Mean $\log_{10}$ changes (±SEM) in serum HCV RNA are plotted. The solved equation described in Methods was fitted to the values in the 8 h group (solid line), and the estimated efficacy and virion clearance rates were 0.992 (95 % CI 0.982–1.00) and 0.200 (95 % CI 0.110–0.291), respectively.

infected and harbour approximately ten HCV genomes per cell at baseline steady state and a 2 $\log_{10}$-fold reduction is achieved with drug treatment.

Mathematical models have proven valuable in understanding the *in vivo* dynamics of HCV, and very rapid dynamic processes occur on timescales of hours to days, and slower processes occur on timescales of weeks to months (Perelson & Ribeiro, 2008). In the last experiment, we observed a biphasic decline in the HCV RNA level after BID dosing for 3 days. During the first 2 days of the treatment, a discrepancy in viral kinetics between the serum-sampling time points was noted. Similarly, fluctuations in viral kinetics during the first-phase slope were observed in patients who received IFN three times a week (Pawlotsky *et al.*, 2004). Variable efficacy rate determined by PK parameters can explain fluctuations during the first-phase slope in mathematical model analysis (Talal *et al.*, 2006). However, it is difficult to evaluate the individual temporal changes in viral and drug kinetics using a mouse model as only a limited volume of blood is available for analysis. Therefore, we assumed a constant efficacy rate (ε) and omitted a turnover rate of hepatocytes because of the short duration of treatment. The estimated clearance rate (c) in this study was 4.8 day^{-1}. Additionally, the mean slope of 0.144 $\log_{10}$ h^{-1} (Fig. 2b) could be transformed to 0.332 h^{-1}=8.0 day^{-1} according to the change of base of a logarithm. The estimated clearance rates in this mouse model basically agreed with estimates determined in humans infected with HCV genotype 1 and undergoing IFN-based therapies (Herrmann *et al.*, 2003; Neumann *et al.*, 1998; Pawlotsky *et al.*, 2004) or large-volume plasma apheresis (Ramratnam *et al.*, 1999). Total virion production during steady-state viral kinetics in this mouse model was calculated by multiplying c by the initial viral load (V_0) and then normalizing the extracellular fluid volume. From previous studies, it was determined that 10^{11}–10^{13} virions are produced daily in patients with high HCV loads (Neumann *et al.*, 1998; Ramratnam *et al.*, 1999). In this mouse model, the volume of extracellular fluid and weight of the liver were approximately 20 and 9% of the body weight (data not shown), and the mean $\log_{10}$ V_0 ($\pm$SEM) among the mice with mean clearance rates of 4.8 and 8.0 per day were 6.96$\pm$0.26 and 7.00$\pm$0.33, respectively. The results of the calculations indicated that 1 g of the chimeric human liver produced 1×10^8–2×10^8 virions per day. The typical weight of the human liver is 1–2 kg; thus, the capacity of human hepatocytes to produce HCV in this mouse model may be equivalent to that in CHC patients. In conclusion, a mouse model with a chimeric human liver can simulate HCV replication in human patients quantitatively and dynamically, and this mouse model may be suitable for preclinical evaluations of novel HCV-specific agents and other therapeutic strategies, including combination regimens.

METHODS

Generation of mice with chimeric human livers and HCV infection. The generation of uPA$^{+/+}$/SCID$^{+/+}$ mice and transplantation of frozen human hepatocytes was performed at PhoenixBio. Graft function was monitored on the basis of HSA levels in blood (Tsuge *et al.*, 2005). All the mice had high HSA levels, which suggested that nearly half of their livers were repopulated by human hepatocytes (Tateno *et al.*, 2004). After obtaining written informed consent, we collected sera periodically from patients who were chronically infected with HCV genotype 1b and failed to respond to PEG-IFN and RBV therapy. The mice were inoculated with the serum samples via the orbital vein after anaesthetization. The experimental protocol was approved by the Ethics Review Committee for Animal Experimentation of the Graduate School of Biomedical Sciences, Hiroshima University.

Compound preparation and experimental designs. The telaprevir formulations were kindly provided by Vertex Pharmaceuticals. A telaprevir suspension was prepared as described previously (Perni *et al.*, 2006) and used in experiments 1 and 2. In the other experiments, a telaprevir suspension was prepared daily as in the tablet formulation (Forestier *et al.*, 2007; Hézode *et al.*, 2009; McHutchison *et al.*, 2009). A suspension of telaprevir was administered via oral gavage.

Experiment 1: preliminary dose-finding study. Ten out of 11 mice developed serum HCV loads greater than 10^4 copies ml^{-1}. Nine mice with high viral loads (>10^5 copies ml^{-1}) were randomized and administered 10 or 100 mg telaprevir kg^{-1} BID or TID over three periods. During period 1, the mice were administered 100 (n=4) or 10 (n=4) mg telaprevir kg^{-1} or vehicle (n=1) BID at 18:00 and 10:00 h for 7 days, and serum samples were collected before treatment and 1 h after administration in the morning on the third and/or seventh day. During period 2, the mice were administered 100 (n=5) or 10 (n=4) mg telaprevir kg^{-1} TID for 3 days, and serum samples were collected before treatment and 4 h after administration of the last dose. Three mice died between periods 2 and 3. During period 3, the mice were administered 100 (n=3) or 10 (n=3) mg telaprevir kg^{-1} TID for 10 days. The mice were sacrificed 5 h after administration of the last dose, and plasma, serum and liver samples were collected.

Experiment 2: evaluation of HCV turnover. Eleven mice were infected with HCV and eight mice survived for more than 15 weeks with steady-state and high viral loads (10^6–10^8 copies ml^{-1}). Six of the mice were administered 200 mg telaprevir kg^{-1} TID at 9:00, 14:00 and 19:00 h for 4 days. On day 1, serum samples were collected before dose administration, 4 h after the first and second doses were administered, and 2 h after the third dose was administered (n=2 each). On day 2, serum samples were collected 1 h after each of the three doses was administered (n=2 each). Serum samples were also collected 4 h after the first and second doses were administered on day 3 (n=3 each) and 4 h after the second dose was administered on day 4.

Experiment 3: PK analysis. After a washout period, six mice from experiment 2 were administered 100 or 300 mg telaprevir kg^{-1} (n=3 each) BID at 19:00 and 9:00 h for 4 days. Serum samples were collected before dose administration, 4 (n=1) or 8 (n=2) h after administration of the second dose, and 5 h after every two doses were administered. After the final dose was administered, plasma for PK analysis was collected at 1 and 4 h. The mice were sacrificed at 8 h, and serum, plasma and liver samples were collected.

Experiment 4: dose dependence and PK/PD analysis. Thirty-six mice were infected with HCV and 13 survived for more than 13 weeks. The median survival time of this cohort was 81 days after infection. Twelve HCV-infected mice were randomized into three groups (A–C; n=4 each) and underwent two periods of BID dosing for 5 days, which were separated by 1-week washout periods. During the first period, the mice in groups A, B and C were administered 300 mg telaprevir kg^{-1}, 100 mg telaprevir kg^{-1} and vehicle,

respectively. Because two mice in group A and two mice in group C died before the second period, two remaining mice in group C and one back-up mouse were assigned to group A (n=2) and group B (n=1). During the second period, mice that received high or low doses were crossed over to the alternative treatment. Serum samples were collected before the first dose was administered and 5 h after every two doses were administered. Plasma samples were also collected at the same time on days 1, 3 and 5 in the first period and days 1, 3 and 4 in the second period. The mice were sacrificed 8 h after administration of the final dose, and serum, plasma and liver samples were collected.

Experiment 5: viral kinetics with BID dosing After infection of 45 mice, 12 HCV-infected mice maintained steady-state and high viral loads (1.2×10^6–8.5×10^7 copies ml^{-1}) for more than 6 months. The median survival time of this cohort was 131 days after infection. These mice were treated with 200 mg telaprevir kg^{-1} BID at 19:00 and 9:00 h for 3 days. The mice were divided into two groups and serum samples were collected just before the second dose was administered and 4 (n=6) or 8 (n=6) h after every two doses were administered.

Serum RNA extraction and HCV RNA quantification. HCV RNA was isolated from 10 μl serum under denaturing conditions using a SepaGene RV-R kit (Sanko Junyaku). The dried precipitates were dissolved in 10 μl diethylpyrocarbonate-treated water. Extracts were duplicated and assayed by quantitative real-time RT-PCR using TaqMan EZ RT-PCR core reagents (Applied Biosystems). Nucleotide positions of the probe and primer sets refer to HCV H77 strain (GenBank accession no. AF009606). The TaqMan probe 5′-6-FAM-CTGCGGAACCGGTGAGTACAC-BHQ-1-3′ (nt 148–168) was purchased from Biosearch Technologies, and the forward (5′-CGGGAGAGCCATAGTGG-3′; nt 130–146) and reverse (5′-AGTACCACAAGGCCTTTCG-3′; nt 272–290) primers were purchased from Sigma-Aldrich. The 25 μl RT-PCR mixture contained 0.2 nmol forward and reverse primers ml^{-1}, 0.3 nmol TaqMan probe ml^{-1} and 5 μl extracted RNA, and was monitored using a PRISM 7900HT sequence detection system (Applied Biosystems). The thermal profile was 2 min at 50 °C, 30 min at 60 °C for reverse transcription and 5 min at 95 °C, followed by 45 cycles of 20 s at 95 °C and 1 min at 62 °C. The HCV replicon I_{389}neo/NS3-3′/5.1 (Lohmann *et al.*, 1999) RNA was transcribed *in vitro* using a T7 RiboMax Express Large Scale RNA Production System (Promega) and purified twice using gel filtration. The concentration of this transcribed RNA was determined by absorbance at 260 nm and serially diluted 10-fold to prepare a standard curve for each assay.

Liver RNA extraction and HCV RNA quantification. A Wizard SV total RNA Isolation System (Promega) was used to obtain a DNase I-treated total RNA sample. The total RNA concentration was determined by absorbance at 260 nm. Total RNA samples were assayed by duplex real-time RT-PCR for relative quantification of HCV RNA using endogenous control gene expression of human β_2-microglobulin (hβ_2m; GenBank accession no. NM_004048), the TaqMan probe 5′-CAL Fluor Orange 560-AGTGGGATCG-AGACATGTAAGCAGCATCAT-BHQ-1-3′ (nt 401–430), and the forward and reverse primer set of 5′-TTGTCACAGCCCAA-GATAGTT-3′ (nt 379–399) and 5′-TGCGGCATCTTCAAACC-3′ (nt 434–450). To adjust the efficacy of PCR amplification of both target genes, the reaction condition was modified from the HCV single-probe assay. The temperature for extension was 60 °C, the concentration of the HCV probe was 0.24 nmol ml^{-1} and the reaction mixture contained the TaqMan probe/primer set for hβ_2m: 0.2 nmol primers ml^{-1} and 0.12 nmol TaqMan probe ml^{-1}. Because both target genes double after one cycle of PCR, a difference in Ct between HCV and hβ2m ($\Delta Ct = Ct_{HCV} - Ct_{h\beta 2m}$) theoretically indicates a relative quantity of HCV RNA per control gene expression of $2^{-\Delta\Delta Ct}$.

Determination of drug concentration. Plasma and liver samples were analysed using chiral liquid chromatography followed by tandem mass spectrometry. After reconstitution, sample extracts were separated by normal-phase chromatography on a 2 × 250 mm Hypersil CPS-1 column (Thermo Hypersil-Keystone) with a mobile phase of heptane : acetone : methanol (82 : 17 : 1). Analyte concentrations were determined by turbo ion spray liquid chromatography/tandem mass spectrometry in the positive-ion mode. Analysis was performed at SRL or Mitsubishi Chemical Medience.

Statistical analysis. The HCV RNA level in serum was normalized by logarithmic conversion. Statistical analysis was performed with a mixed linear model using SAS (SAS Institute). Mean differences between two groups were evaluated with Student's t-test. The difference compared with vehicle control at each time point was evaluated by Dunnett's multiple comparisons test. Linear and non-linear regression analyses were performed using GraphPad Prism 5 (GraphPad Software).

Viral dynamics model analysis. The basic mathematical model for the analysis of HCV infection *in vivo*, which is a system of three ordinary differential equations for uninfected cells (T), productively infected cells (I) and free virus (V), has been reviewed elsewhere (Perelson & Ribeiro, 2008). Briefly, one of the three equations ($dV/dt = pI - cV$), where viral particles are produced at rate p per infected cell and cleared at rate c per virion, was solved. During treatment for 2–3 days, if one assumes that the number of I is approximately constant and equal to its pre-treatment value and that the viral level was at its set-point value (V_0), then $pI = cV_0$. Using this relationship in the equation $dV/dt = (1-\varepsilon)pI - cV$, where ε is the effectiveness in blocking virion production, yields $dV/dt = (1-\varepsilon)\,cV_0 - cV$, $V(0) = V_0$ with the solution $V(t) = V_0(1 - \varepsilon + \varepsilon e^{-ct})$. Because the log change of viral load at time [$\log \Delta V(t)$] equals $\log V(t)/V_0$, the solved equation [$\log \Delta V(t) = \log(1 - \varepsilon + \varepsilon e^{-ct})$] was fitted to the values obtained in this study via non-linear least-squares regression in order to estimate ε and c.

ACKNOWLEDGEMENTS

We thank Drs Ichimaro Yamada, Mitsubishi Tanabe Pharma Corporation, and Ann D Kwong, Gururaj Kalkeri, Susan Almquist, Steven M. Lyons and John Randle, Vertex Pharmaceuticals, for their thoughtful discussions. This work was supported in part by Grants-in-Aid for scientific research and development from the Ministry of Education, Sports, Culture and Technology and the Ministry of Health, Labour and Welfare, Japan.

REFERENCES

Boonstra, A., van der Laan, L. J. W., Vanwolleghem, T., Harry, L. A. & Janssen, H. L. A. (2009). Experimental models for hepatitis C viral infection. *Hepatology* **50**, 1646–1655.

Chang, M., Williams, O., Mittler, J., Quintanilla, A., Carithers, R. L., Jr, Perkins, J., Corey, L. & Gretch, D. R. (2003). Dynamics of hepatitis C virus replication in human liver. *Am J Pathol* **163**, 433–444.

Dahari, H., Feliu, A., Garcia-Retortillo, M., Forns, X. & Neumann, A. U. (2005). Second hepatitis C replication compartment indicated by viral dynamics during liver transplantation. *J Hepatol* **42**, 491–498.

Forestier, N., Reesink, H. W., Weegink, C. J., McNair, L., Kieffer, T. L., Chu, H.-M., Purdy, S., Jansen, P. L. M. & Zeuzem, S. (2007). Antiviral

activity of telaprevir (VX-950) and peginterferon alfa-2a in patients with hepatitis C. *Hepatology* **46**, 640–648.

Fried, M. W., Shiffman, M., Reddy, K. R., Smith, C., Marinos, G., Gonçales, F. L., Jr, Häussinger, D., Diago, M., Carosi, G. & other authors (2002). Peginterferon alfa-2a plus ribavirin for chronic hepatitis C virus infection. *N Engl J Med* **347**, 975–982.

Herrmann, E., Lee, J.-H., Marinos, G., Modi, M. & Zeuzem, S. (2003). Effect of ribavirin on hepatitis C viral kinetics in patients treated with pegylated interferon. *Hepatology* **37**, 1351–1358.

Hézode, C., Forestier, N., Dusheiko, G., Ferenci, P., Pol, S., Goeser, T., Bronowicki, M., Bourlière, J.-P., Gharakhanian, S. & other authors (2009). Telaprevir and peginterferon with or without ribavirin for chronic HCV infection. *N Engl J Med* **360**, 1839–1850.

Hiraga, N., Imamura, M., Tsuge, M., Noguchi, C., Takahashi, S., Iwao, E., Fujimoto, Y., Abe, H., Maekawa, T. & other authors (2007). Infection of human hepatocyte chimeric mouse with genetically engineered hepatitis C virus and its susceptibility to interferon. *FEBS Lett* **581**, 1983–1987.

Katoh, M., Sawada, T., Soeno, Y., Nakajima, M., Tateno, C., Yoshizato, K. & Yokoi, T. (2007). *In vivo* drug metabolism model for human cytochrome P450 enzyme using chimeric mice with humanized liver. *J Pharm Sci* **96**, 428–437.

Katoh, M., Tateno, C., Yoshizato, K. & Yokoi, T. (2008). Chimeric mice with humanized liver. *Toxicology* **246**, 9–17.

Kimura, T., Imamura, M., Hiraga, N., Hatakeyama, T., Miki, D., Noguchi, C., Mori, N., Tsuge, M., Takahashi, S. & other authors (2008). Establishment of an infectious genotype 1b hepatitis C virus clone in human hepatocyte chimeric mice. *J Gen Virol* **89**, 2108–2113.

Kneteman, N. M., Weiner, A. J., O'Connell, J., Collett, M., Gao, T., Aukerman, L., Kovelsky, R., Ni, Z.-J., Hashash, A. & other authors (2006). Anti-HCV therapies in chimeric *scid*-Alb/uPA mice parallel outcomes in human clinical application. *Hepatology* **43**, 1346–1353.

Kneteman, N. M., Howe, A. Y. M., Gao, T., Lewis, J., Pevear, D., Lund, G., Douglas, D., Mercer, D. F., Tyrrell, D. L. J. & other authors (2009). HCV796: a selective nonstructural protein 5B polymerase inhibitor with potent anti-hepatitis C virus activity *in vitro*, in mice with chimeric human livers, and in humans infected with hepatitis C virus. *Hepatology* **49**, 745–752.

Lauer, G. M. & Walker, B. D. (2001). Hepatitis C virus infection. *N Engl J Med* **345**, 41–52.

Liang, T. J., Rehermann, B., Seeff, L. B. & Hoofnagle, J. H. (2000). Pathogenesis, natural history, treatment and prevention of hepatitis C. *Ann Intern Med* **132**, 296–305.

Lindenbach, B. D., Meuleman, P., Ploss, A., Vanwolleghem, T., Syder, A. J., McKeating, J. A., Lanford, R. E., Feinstone, S. M., Major, M. E. & other authors (2006). Cell culture-grown hepatitis C virus is infectious *in vivo* and can be recultured *in vitro*. *Proc Natl Acad Sci U S A* **103**, 3805–3809.

Lohmann, V., Körner, F., Koch, J., Herian, U., Theilmann, L. & Bartenschlager, R. (1999). Replication of subgenomic hepatitis C virus RNAs in a hepatoma cell line. *Science* **285**, 110–113.

Manns, M. P., McHutchison, J. G., Gordon, S. C., Rustgi, V. K., Shiffman, M., Reindollar, R., Goodman, Z. D., Koury, K., Ling, M.-H. & other authors (2001). Peginterferon alfa-2b plus ribavirin compared with interferon alfa-2b plus ribavirin for initial treatment of chronic hepatitis C: a randomised trial. *Lancet* **358**, 958–965.

Manns, M. P., Foster, G. R., Rockstroh, J. K., Zeuzem, S., Zoulim, F. & Houghton, M. (2007). The way forward in HCV treatment – finding the right path. *Nat Rev Drug Discov* **6**, 991–1000.

McHutchison, J. G., Everson, G. T., Gordon, S. C., Jacobson, I. M., Sulkowski, M., Kauffman, R., McNair, L., Alam, J., Muir, A. J. & other authors (2009). Telaprevir with peginterferon and ribavirin for chronic HCV genotype 1 infection. *N Engl J Med* **360**, 1827–1838.

Mercer, D. F., Schiller, D. E., Elliott, J. F., Douglas, D. N., Hao, C., Rinfret, A., Addison, W. R., Fischer, K. P., Churchill, T. A. & other authors (2001). Hepatitis C virus replication in mice with chimeric human livers. *Nat Med* **7**, 927–933.

Neumann, A. U., Lam, N. P., Dahari, H., Gretch, D. R., Wiley, T. E., Layden, T. J. & Perelson, A. S. (1998). Hepatitis C viral dynamics *in vivo* and the antiviral efficacy of interferon-α therapy. *Science* **282**, 103–107.

Pawlotsky, J.-M., Dahari, H., Neumann, A. U., Hezode, C., Germanidis, G., Lonjon, I., Castera, L. & Dhumeaux, D. (2004). Antiviral action of ribavirin in chronic hepatitis C. *Gastroenterology* **126**, 703–714.

Pereira, A. A. & Jacobson, I. M. (2009). New and experimental therapies for HCV. *Nat Rev Gastroenterol Hepatol* **6**, 403–411.

Perelson, A. S. & Ribeiro, R. M. (2008). Estimating drug efficacy and viral dynamic parameters: HIV and HCV. *Stat Med* **27**, 4647–4657.

Perni, R. B., Almquist, S. J., Byrn, R. A., Chandorkar, G., Chaturvedi, P. R., Courtney, L. F., Decker, C. J., Dinehart, K., Gates, C. A. & other authors (2006). Preclinical profile of VX-950, a potent, selective, and orally bioavailable inhibitor of hepatitis C virus NS3-4A serine protease. *Antimicrob Agents Chemother* **50**, 899–909.

Powers, K. A., Ribeiro, R. M., Patel, K., Pianko, S., Nyberg, L., Pockros, P., Conrad, A. J., McHutchison, J. & Perelson, A. S. (2006). Kinetics of hepatitis C virus reinfection after liver transplantation. *Liver Transpl* **12**, 207–216.

Poynard, T., Yuen, M.-F., Ratziu, V. & Lai, C. L. (2003). Viral hepatitis C. *Lancet* **362**, 2095–2100.

Quinkert, D., Bartenschlager, R. & Lohmann, V. (2005). Quantitative analysis of the hepatitis C virus replication complex. *J Virol* **79**, 13594–13605.

Ramratnam, B., Bonhoeffer, S., Binley, J., Hurley, A., Zhang, L., Mittler, J. E., Minarkowitz, M., Moore, J. P., Perelson, A. S. & Ho, D. D. (1999). Rapid production and clearance of HIV-1 and hepatitis C virus assessed by large volume plasma apheresis. *Lancet* **354**, 1782–1785.

Reesink, H. W., Zeuzem, S., Weegink, C. J., Forestier, N., Vliet, A., van de Wetering de Rooij,, J., McNair, L., Purdy, S., Kauffman, R. & other authors (2006). Rapid decline of viral RNA in hepatitis C patients treated with VX-950: a phase Ib, placebo-controlled, randomized study. *Gastroenterology* **131**, 997–1002.

Sarrazin, C., Kieffer, T. L., Bartels, D., Hanzelka, B., Möh, U., Welker, M., Wincheringer, D., Zhou, Y., Chu, H.-M. & other authors (2007). Dynamic hepatitis C virus genotypic and phenotypic changes in patients treated with the protease inhibitor telaprevir. *Gastroenterology* **132**, 1767–1777.

Schiano, T. D., Gutierrez, J. A., Walewski, J. L., Fiel, M. I., Cheng, B., Bodenheimer, H., Jr, Thung, S. N., Chung, R. T., Schwartz, M. E. & other authors (2005). Accelerated hepatitis C virus kinetics but similar survival rates in recipients of liver grafts from living versus deceased donors. *Hepatology* **42**, 1420–1428.

Sherman, K. E., Fleischer, R., Laessig, K., Murray, J., Tauber, W. & Birnkrant, D. (2007). Development of novel agents for the treatment of chronic hepatitis C infection: summary of the FDA antiviral products advisory committee recommendations. *Hepatology* **46**, 2014–2020.

Talal, A. H., Ribeiro, R. M., Powers, K. A., Grace, M., Cullen, C., Hussain, M., Markatou, M. & Perelson, A. S. (2006). Pharmacodynamics of PEG-IFN α differentiate HIV/HCV coinfected sustained virological responders from nonresponders. *Hepatology* **43**, 943–953.

Tateno, C., Yoshizane, Y., Saito, N., Kataoka, M., Utoh, R., Yamasaki, C., Tachibana, A., Soeno, Y., Asahina, K. & other authors (2004). Near completely humanized liver in mice shows human-type metabolic responses to drugs. *Am J Pathol* **165**, 901–912.

Tsuge, M., Hiraga, N., Takaishi, H., Noguchi, C., Oga, H., Imamura, M., Takahashi, S., Iwao, E., Fujimoto, Y. & other authors (2005). Infection of human hepatocyte chimeric mouse with genetically engineered hepatitis B virus. *Hepatology* **42**, 1046–1054.

Vanwolleghem, T., Meuleman, P., Libbrecht, L., Roskams, T., De Vos, R. & Leroux-Roels, G. (2007). Ultra-rapid cardiotoxicity of the hepatitis C virus protease inhibitor BILN 2061 in the urokinase-type plasminogen activator mouse. *Gastroenterology* **133**, 1144–1155.

Vona, G., Tuveri, R., Delpuech, O., Vallet, A., Canioni, D., Ballardini, G., Trabut, J. B., Le Bail, B., Nalpas, B. & other authors (2004). Intrahepatic hepatitis C virus RNA quantification in microdissected hepatocytes. *J Hepatol* **40**, 682–688.

Wasley, A. & Alter, M. J. (2000). Epidemiology of hepatitis C: geographic differences and temporal trends. *Semin Liver Dis* **20**, 1–16.

THE JOURNAL OF GENE MEDICINE
J Gene Med 2010;12: 1002–1013.
Published online in Wiley Online Library (wileyonlinelibrary.com) DOI: 10.1002/jgm.1528

RESEARCH ARTICLE

Prevention of intrahepatic metastasis of liver cancer by suicide gene therapy and chemokine ligand 2/monocyte chemoattractant protein-1 delivery in mice

Kaheita Kakinoki[1]
Yasunari Nakamoto[1]
Takashi Kagaya[1]
Tomoya Tsuchiyama[1]
Yoshio Sakai[1]
Tohru Nakahama[1]
Naofumi Mukaida[2]
Shuichi Kaneko[1]*

[1]*Disease Control and Homeostasis, Graduate School of Medical Science, Kanazawa University, Kanazawa, Japan*

[2]*Division of Molecular Bioregulation, Cancer Research Institute, Kanazawa University, Kanazawa, Japan*

*Correspondence to:
Shuichi Kaneko, Disease Control and Homeostasis, Graduate School of Medical Science, Kanazawa University, 13-1 Takara-machi, Kanazawa 920-8641, Japan
E-mail: skaneko@m-kanazawa.jp

Received: 22 June 2010
Revised: 28 October 2010
Accepted: 5 November 2010

Abstract

Background The prognosis of patients with hepatocellular carcinoma (HCC) remains poor, largely as a result of intrahepatic metastasis. Using a mouse model of intrahepatic metastasis, we investigated whether chemokine ligand 2/monocyte chemoattractant protein-1 (CCL2/MCP-1) could potentiate the antitumor effects of the herpes simplex virus thymidine kinase/ganciclovir (HSV-tk/GCV) system.

Methods Mouse hepatoma cells infected with recombinant adenovirus vectors expressing HSV-tk, CCL2/MCP-1 and LacZ at multiplicities of infection of Ad-tk/Ad-MCP1 = 3/0.03 (T/M^{Low}), 3/3 (T/M^{High}) and Ad-tk/Ad-LacZ = 3/3 (T/L) were injected into BALB/c mice.

Results Intrahepatic tumor growth was significantly lower in T/M^{Low} mice. By contrast, no tumor suppression was observed in T/M^{High} mice. The tumor-specific cytolytic activities of splenocytes from T/M^{Low} and T/M^{High} mice were comparable. Immunohistochemical analysis of liver tissues showed similar infiltration by Mac-1^+ and T cells in these animals, whereas the proportions of classical activated (M1) monocytes/macrophages were significantly higher in T/M^{Low} mice. In addition, interleukin-12 production was elevated in these tissues. Vascular endothelial growth factor-A expression and $CD31^+$ microvessels were increased in T/M^{High} mice.

Conclusions Collectively, these results demonstrate that an adequate amount of CCL2/MCP-1, together with the HSV-tk/GCV system, may induce T helper 1-polarized antitumor effects without inducing tumor angiogenesis in the microenvironment of intrahepatic HCC progression. Copyright © 2010 John Wiley & Sons, Ltd.

Keywords chemokines; hepatocellular carcinoma; monocytes/macrophages

Introduction

Primary liver cancer is the fifth most common neoplasm in the world and the third most common cause of cancer-related deaths [1,2]. Despite the development of novel modalities for the treatment of hepatocellular carcinoma (HCC), including transcatheter arterial embolization, percutaneous ablation, surgical resection and liver transplantation, the prognosis of patients with HCC still remains relatively poor. One of the major factors responsible for

Copyright © 2010 John Wiley & Sons, Ltd.